

Optical spectroscopy of two overlapping, flux-density–limited samples of radio sources in the North Ecliptic Cap, selected at 38 MHz and 151 MHz

Mark Lacy¹ \star , Steve Rawlings¹, Gary J. Hill², Andrew J. Bunker³, Susan E. Ridgway^{1,4} & Daniel Stern³

¹*Astrophysics, Department of Physics, Keble Road, Oxford, OX1 3RH.*

²*McDonald Observatory, University of Texas at Austin, TX78712-1083*

³*Dept of Astronomy, University of California at Berkeley, 601 Campbell Hall, Berkeley CA 94720*

⁴*Bloomberg Center for Physics & Astronomy, Johns Hopkins University, 3400 Charles Street, Baltimore MD 21218*

24 March 2019

ABSTRACT

We present the results of optical spectroscopy of two flux-density–limited samples of radio sources selected at frequencies of 38 and 151 MHz in the same region around the North Ecliptic Cap, the 8C-NEC and 7C-III samples respectively. Both samples are selected at flux density levels ≈ 20 times fainter than samples based on the 3C catalogue. They are amongst the first low-frequency selected samples with no spectral or angular size selection for which almost complete redshift information has been obtained, and contain many of the lowest-luminosity $z > 2$ radio galaxies so far discovered. They will therefore provide a valuable resource for understanding the cosmic evolution of radio sources and their hosts and environments. The 151-MHz 7C-III sample is selected to have $S_{151} \geq 0.5\text{Jy}$ and is the more spectroscopically complete; out of 54 radio sources fairly reliable redshifts have been obtained for 44 objects. The 8C sample has a flux limit of $S_{38} \geq 1.3\text{Jy}$ and contains 58 sources of which 46 have fairly reliable redshifts. We discuss possible biases in the observed redshift distribution, and some interesting individual objects, including a number of cases of probable gravitational lensing. Using the 8C-NEC and 7C-III samples in conjunction, we form the first sample selected on low-frequency flux in the rest-frame of the source, rather than the usual selection on flux density in the observed frame. This allows us to remove the bias associated with an increasing rest-frame selection frequency with redshift. We investigate the difference this selection makes to correlations of radio source properties with redshift and luminosity by comparing the results from traditional flux-density selection with our new method. We show in particular that flux-density–based selection leads to an overestimate of the steepness of the correlation of radio source size with redshift.

Key words: galaxies: active – galaxies: evolution – radio continuum: galaxies – gravitational lensing

1 INTRODUCTION

Spectroscopic surveys of radio sources at flux density levels much lower than those of the 3C catalogue and its various revisions (e.g. Laing, Riley & Longair 1983, hereafter LRL) are essential to provide coverage of the redshift–radio luminosity plane. Such coverage is required to establish the cosmic evolution of these sources both in number density and physical properties such as size and structure. Over the past two

decades, several flux-limited samples selected at low radio frequency (and hence directly comparable with LRL in being selected primarily on the basis of unbeamed steep spectrum radio lobe emission) have been defined and imaged in the radio and optical. Only recently, however, have redshifts have been obtained for a significant fraction of the radio sources. This paper describes spectroscopic observations of the 38-MHz 8C North Ecliptic Cap (NEC) sample of Lacy, Rawlings & Warner (1992; hereafter Paper I) and Lacy et al. 1993, 1999a (hereafter Papers II and III respectively), and the closely-related 7C-III sample. This latter sample was se-

\star email: m.lacy1@physics.oxford.ac.uk

lected at a frequency of 151 MHz using the 7C survey data of Lacy et al. (1995) with a flux limit chosen to maximise overlap with the 8C sample. This sample is defined in Section 2, and will be described in more detail in a future paper (Lacy et al. 1999b). A further paper will discuss spectroscopy of the 6C sample of Eales (1985), and details of the 7C-I and 7C-II samples are presented in Willott (1998, and papers in preparation). The properties of these samples are summarised in Table 1, and the coverage of the radio-luminosity – redshift plane is illustrated in, e.g. fig. 1 of Blundell, Rawlings & Willott (1999).

Samples such as these are very valuable for studying the cosmic evolution of the radio source population, in particular the question of the evolution of source size, D , with redshift. As redshift and radio luminosity are always strongly correlated within any flux-limited sample, partial correlation coefficients need to be calculated to investigate whether the true correlation is with redshift or luminosity. Studies based on low-frequency selected samples typically show a weak correlation with redshift only, parameterised as $D \propto (1+z)^{-\eta}$ where $\eta \approx 1.7 - 1.9$ (e.g. the 6C sample, Eales 1985; Neeser et al. 1995, and the 7C-I and 7C-II samples; Blundell, Rawlings & Willott 1999), although samples selected at higher frequencies seem to have stronger dependences, with $\eta \approx 3$ (Oort, Katgert & Windhorst 1987; Kapahi 1989) combined with a radio luminosity dependence $D \propto L^\epsilon$ with $\epsilon \approx 0.3$.

In Paper II we performed a partial rank correlation on the 8C-NEC sample using photometric redshifts. This showed that the fundamental correlation was between size and redshift, but having only redshifts based on R -band magnitudes we were forced to only consider $z < 1.1$ objects and to accept the uncertainties associated with photometric redshifts. We also investigated the four-way correlation coefficients of redshift, luminosity, size and spectral index, finding that spectral index at 2GHz in the rest frame was most strongly correlated with redshift, and any correlation with luminosity was weak. Since then, independent work on the 6C, 7C-I and 7C-II surveys has been carried out by Blundell et al. (1999) with results that are broadly consistent with the Neeser et al. result and the results of Paper II. They find, however, a significant correlation of spectral index with luminosity at a rest-frame frequency of 1 GHz, although a correlation with redshift is seen at higher frequencies. In this paper we use the redshifts for the 7C-III and 8C-NEC samples to study the size-redshift relation further.

We assume $H_0 = 50 \text{ kms}^{-1} \text{ Mpc}^{-1}$ and an Einstein – de Sitter ($\Omega_M = 1$, $\Omega_\Lambda = 0$) cosmology unless otherwise stated. Positions are all epoch B1950.0. Spectral indices, both radio and optical are defined in the sense that $S_\nu \propto \nu^{-\alpha}$.

2 SAMPLE DEFINITIONS AND THE SPECTROSCOPIC SUB-SAMPLES

The 8C-NEC sample has been formally defined in Paper I, and some refinements described in Paper III. It consists of all radio sources with 38-MHz flux densities $S_{38} \geq 1.3 \text{ Jy}$ within 3° of $18^{\text{h}}00^{\text{m}} +66^\circ$ in the survey of Rees (1990). The 7C-III sample consists of all 7C objects from the mini-survey of Lacy et al. (1995) with 151-MHz flux densities $S_{151} \geq 0.5 \text{ Jy}$, again within 3° of $18^{\text{h}}00^{\text{m}} +66^\circ$. The flux density lim-

Table 1. Complete, flux-density limited radio source samples at low radio frequency selected from the Cambridge surveys for which optical spectra have been obtained

Name	Selection criteria
6C	$2 < S_{151} < 4 \text{ Jy}$, $8^{\text{h}}20^{\text{m}} < \text{R.A.} < 13^{\text{h}}01^{\text{m}}$, $34^\circ < \text{Dec.} < 40^\circ$
7C-I	$S_{151} \geq 0.5 \text{ Jy}$ in the 5C6 field
7C-II	$S_{151} \geq 0.5 \text{ Jy}$ in the 5C7 field
7C-III	54 sources with $S_{151} \geq 0.5 \text{ Jy}$ within 3° of the NEC [for maximum overlap with the 8C NEC sample]
8C-NEC	58 sources with $S_{38} \geq 1.3 \text{ Jy}$ within 3° of the NEC

its are deliberately chosen to maximise the overlap of the two samples, thus most sources are common to both samples. The 7C-III sample will be more fully described in Lacy et al. 1999b, but the positions and radio properties of the objects which are present only in the 7C-III sample (and which therefore have not appeared in Papers I-III) are presented in Table 2, for completeness. A number of objects have been excluded from the samples on the basis of confusion by bright nearby sources. 7C 1732+6715 (8C 1732+672) has a very bright radio source nearby and has been temporarily removed from the sample pending an improved radio image. 7C 1821+6442 (8C 1821+646) has a star on top of the ID position (R.G. McMahon, personal communication). 7C 1827+6517 (8C 1827+652) has been excluded as there is a very bright star nearby. This has reduced the total number of objects in the 7C-III sample from 57 to 54 and for the 8C-NEC sample from 61 to 58. As these objects were removed for reasons unconnected with their intrinsic radio or optical properties their omission should not affect the sample statistics. Apart from these, all objects in the 7C-III sample have spectroscopic data. In the 8C-NEC sample, there are three objects for which spectra are yet to be obtained.

3 SPECTROSCOPIC OBSERVATIONS

Most of the objects in both the 8C-NEC and 7C-III North Ecliptic Cap samples were observed with the ISIS spectrograph on the William Herschel Telescope (WHT). Most observations were made on the nights of 1995 July 28 to 31, though observations of a few objects were made by on the nights of 1993 August 20-21 and 1993 June 18-19. Observations of brighter objects in the sample were made with the IGI on the McDonald Observatory 107" telescope on the nights of 1993 July 27-28. Two objects were observed using the Kast spectrograph on the Shane 3-m telescope at the Lick Observatory. Details of the observations are given in Tables 3 and 5.

In most cases, a long spectroscopic slit was centred on the optical identification and aligned with the radio axis, offsetting from a nearby star (positions of offset stars are available from ML). In a few cases there was no identification on optical or infrared images, in which case the spectrum was taken blind, with the slit aligned along the radio axis.

The ISIS observations were made using both arms and a dichroic at either 540nm (in 1993) or 570nm (in 1995). In 1993 June and August the red and blue arm detectors were an EEV5 CCD and a TEK CCD respectively, in 1995 July

Table 2. Objects in the 7C-III sample which are not in the 8C-NEC sample

Name	S_{151} /Jy	R.A. (1950)	Dec. (1950)	α_{151}^{38}	R	Radio size/''	Radio PA	Notes
7C1731+6641	0.52	17 31 43.57	+66 40 59.3	0.40	21.4	1.0	164	
7C1740+6640	0.54	17 40 42.80	+66 40 07.2	0.37	24.8	<0.5	-	see Section 4.3
7C1745+6624	0.51	17 45 57.20	+66 24 18.5	0.49	-	<0.5	-	see Section 4.3
7C1748+6657	1.15	17 48 17.57	+66 57 15.8	<-0.26	22.4	0.3	90	
7C1807+6719	0.71	18 07 19.56	+67 19 11.6	0.25	>23	1.9	47	
7C1812+6814	0.59	18 12 15.65	+68 14 06.5	0.51	>23	22.0	123	
7C1820+6657	0.83	18 20 40.21	+66 57 12.1	<-0.03	>23	<0.5	-	

Note: positions are those of the optical/IR identification except for 7C1812+6814 where the identification is only seen in the spectrum and 7C1820+6657 which is unidentified optically apart from a very faint emission line in the spectrum. In these cases the radio position has been quoted (this is the mid-point of the hotspots in the case of 7C1812+6814).

both detectors were TEK CCDs. The TEK CCD suffers from fringing at the red end of the red arm, but was preferred to the EEV5 in 1995 because of its higher quantum efficiency. In practice, it proved possible to remove the fringing effectively by taking tungsten lamp flats immediately following each observation, before moving the telescope.

The IGI observations were made as described in Paper II. The Kast observations were made with both red and blue arms, the beam being split by a dichroic at 550 nm. Reticon CCDs were used as detectors in both arms and 452 and 300 lmm⁻¹ gratings were employed in the blue and red arms respectively.

Data reduction of the WHT, 107'' and Lick data followed the standard procedure of bias subtraction, division by a flatfield, wavelength calibration using arc lamp spectra (CuAr and CuNe for the WHT data, Cd for the 107'' data and CdHeHg and NeAr for the Lick data) and flux calibration using spectrophotometric standard stars.

Errors in the spectrophotometry are expected to be \approx 15 per cent; errors in the wavelengths of the bright spectral features are not expected to be larger than 0.2 nm in the WHT and Lick data and 0.3 nm in the McDonald data.

3.1 The 7C-III spectra

In Fig. 1 we present the spectra of the objects in the 7C-III sample with the main spectral features labelled. The WHT spectra in the figure have been smoothed with a 1.5 nm box-car filter, and the McDonald and Lick spectra by a 1.2 nm one. If features appear in only one arm of the WHT spectrum, the other has not been shown. All spectra for objects in the spectroscopic sub-sample are shown except for those already published in Paper II, or Lacy et al. (1999c; hereafter LRWLR), those for which spectra have been published by Kollgaard et al. (1995; hereafter K95) and those for which there are no spectral features visible. These are shown separately in Fig. 2. Derived redshifts and emission line properties (flux, equivalent width and velocity width) are listed in Table 4. The emission line properties are derived from Gaussian fits to the data.

3.2 Spectra of objects in the 8C-NEC sample only

We have also obtained data on some objects in the original 8C-NEC sample of Paper I which were just below the $S_{151} = 0.5$ Jy flux density cutoff of the 7C-III sample. The observations are listed in Table 5 and the redshifts and other

emission line properties in Table 6, with the whole sample listed for completeness. The spectra are shown in Fig. 6, smoothed as in Fig. 1 except for 8C 1758+676 which appears to be a faint quasar, and to which a smoothing of 4 nm has been applied to bring out the broad lines.

4 RESULTS

4.1 Reliability of the redshifts

The redshifts in Tables 4 and 6 come from spectra in which the signal:noise and number of spectral features used to estimate the redshift varied widely. Those which we consider “firm” are based on more than one strong spectral feature (emission or absorption lines or 4000Å break), and are graded α . Those with either one strong spectral feature and one or more low signal:noise ones, or with two or more low signal:noise features are graded β . Those based on a single spectral feature (for emission lines we usually assume to be Ly α if it appears in the blue arm spectrum or [OII]372.7 if it appears in the red), or two very weak features are graded γ , and should be considered unreliable until further data are obtained.

For some objects we have only been able to place an upper bound on the redshift by detecting continuum in the blue arm spectrum. Due to the low transmissivity of Lyman limit systems we can be fairly sure that if, for example, we see continuum to the atmospheric cutoff (340 nm) then the redshift of the radio source is $< 340/91.2 - 1 = 2.7$

4.2 Possible biases in the redshift distribution

There are a number of observational problems which could lead to biases in the measured redshift distribution of objects. The most serious bias probably comes from the difficulty of measuring redshifts for objects with $1.2 < z < 1.8$, where [OII]372.7 moves out of the red arm spectrum, but before Ly α moves into the observable part of the blue. This is borne out by inspection of the redshift distribution which seems deficient in objects with $1.2 < z < 1.8$ compared to the predictions of the Dunlop & Peacock (1990) models (Fig. 3). Measurement of redshifts in this range depends on fainter features, typically MgII 279.8 and CIII]190.9; consequently it is likely that many of the objects with no measured redshift lie in this range. The radio luminosity function derived from the 7C redshift surveys will be discussed in a future paper (Willott et al. 1999).

Table 3. Log of new spectroscopy of the 7C-III radio sources

7C Name	Observing date(s)	Telescope	wavelength range(s)	integration time(s)/sec	slit width /arcseconds	slit PA	airmass
7C 1731+6641	31/07/95	WHT	330 - 850 nm	500R, 650B	3	164	1.27
7C 1732+6715	28/07/95	WHT	330 - 850 nm	300	2	200	1.29
7C 1733+6719	29/07/95	WHT	330 - 850 nm	1800	3	15	1.32
7C 1740+6640	29/07/95	WHT	330 - 850 nm	1800	3	113	1.55
	31/07/95	WHT	330 - 850 nm	1800	3	20	1.34
7C 1741+6704	20/08/93	WHT	330 - 850 nm	1800B, 1700R	3	56	1.44
7C 1742+6346	28/07/95	WHT	330 - 850 nm	1800	3	63	1.22
7C 1743+6431	28/07/95	WHT	330 - 850 nm	1800	3	90	1.53
	29/07/95	WHT	330 - 850 nm	1800	3	88	1.25
7C 1743+6344	30/07/95	WHT	330 - 850 nm	1800	3	10	1.47
7C 1745+6415	31/07/95	WHT	330 - 850 nm	500R, 560B	3	177	1.24
7C 1745+6422	30/07/95	WHT	330 - 850 nm	1280R, 1330B	3	35	1.23
7C 1745+6624	29/07/95	WHT	330 - 850 nm	1800	3	105	1.65
7C 1748+6703	30/07/95	WHT	330 - 850 nm	1800	3	90	1.29
7C 1748+6657	29/07/95	WHT	330 - 850 nm	1650R, 1700B	3	144	1.36
7C 1748+6731	29/07/95	WHT	330 - 850 nm	600	3	0	1.31
7C 1751+6809	30/07/95	WHT	330 - 850 nm	1800	3	31	1.33
7C 1751+6455	27/07/93	107"	430 - 700 nm	3600	2	-	1.25
7C 1753+6311	19/08/93	WHT	330 - 850 nm	1800B, 1700R	3	74	1.60
	31/07/95	WHT	330 - 850 nm	1800	3	70	1.24
7C 1754+6420	28/07/95	WHT	330 - 850 nm	1800	2.5	15	1.23
7C 1755+6314	28/07/93	107"	430 - 700 nm	3600	2	-	1.31
7C 1755+6830	31/07/95	WHT	330 - 850 nm	600	3	65	1.35
7C 1756+6520	30/07/95	WHT	330 - 850 nm	1800	3	47	1.32
7C 1758+6535	29/07/95	WHT	330 - 850 nm	1800	3	52	1.26
7C 1758+6553	28/07/93	107"	430 - 700 nm	1800	2	-	1.52
7C 1758+6307	28/07/95	WHT	330 - 850 nm	900	3	91	1.84
7C 1758+6719	28/07/95	WHT	330 - 850 nm	1800	3	177	1.25
7C 1802+6456	18/06/93	WHT	330 - 850 nm	1800	3	25	1.27
7C 1804+6625	28/07/95	WHT	330 - 850 nm	600	2	206	1.29
7C 1804+6313	31/07/95	WHT	330 - 850 nm	2 × 600	3	47,112	1.26,1.47
7C 1805+6332	20/08/93	WHT	330 - 850 nm	1800	3	0	1.55
7C 1807+6831	29/07/95	WHT	330 - 850 nm	600	3	60	1.32
7C 1807+6719	29/07/95	WHT	330 - 850 nm	1800	3	52	1.26
7C 1807+6841	28/07/95	WHT	330 - 850 nm	1520R, 1600B	3	177	1.30
7C 1811+6321	29/07/95	WHT	330 - 850 nm	600	3	22	1.64
7C 1812+6814	29/07/95	WHT	330 - 850 nm	1800	3	123	1.38
7C 1813+6846	29/07/95	WHT	330 - 850 nm	300	2	0	1.37
7C 1813+6439	05/07/97	Shane	330 - 1060 nm	3600	2	-	1.3
7C 1814+6702	20/08/93	WHT	330 - 900 nm	1800B, 1700R	3	156	1.36
	31/07/95	WHT	330 - 850 nm	1800	2	156	1.36
7C 1814+6529	30/07/95	WHT	330 - 850 nm	1800	3	48	1.25
7C 1815+6815	17/06/93	WHT	330 - 850 nm	1700	3	100	1.31
7C 1816+6710	28/07/95	WHT	330 - 850 nm	1800	3	90	1.60
7C 1816+6605	31/07/95	WHT	330 - 850 nm	1500B, 1450R	2	40	1.27
7C 1819+6550	30/07/95	WHT	330 - 850 nm	1650	3	70	1.51
7C 1820+6657	30/07/95	WHT	330 - 850 nm	1800	3	178	1.37
7C 1822+6601	28/07/93	107"	430 - 700 nm	3600	2	-	1.61
7C 1825+6602	31/07/95	WHT	330 - 850 nm	1800	2-3	78	1.26
7C 1826+6510	28/07/95	WHT	330 - 850 nm	1800	3	123	1.36
7C 1827+6709	28/07/95	WHT	330 - 850 nm	1570B, 1500R	2.5	137	1.34

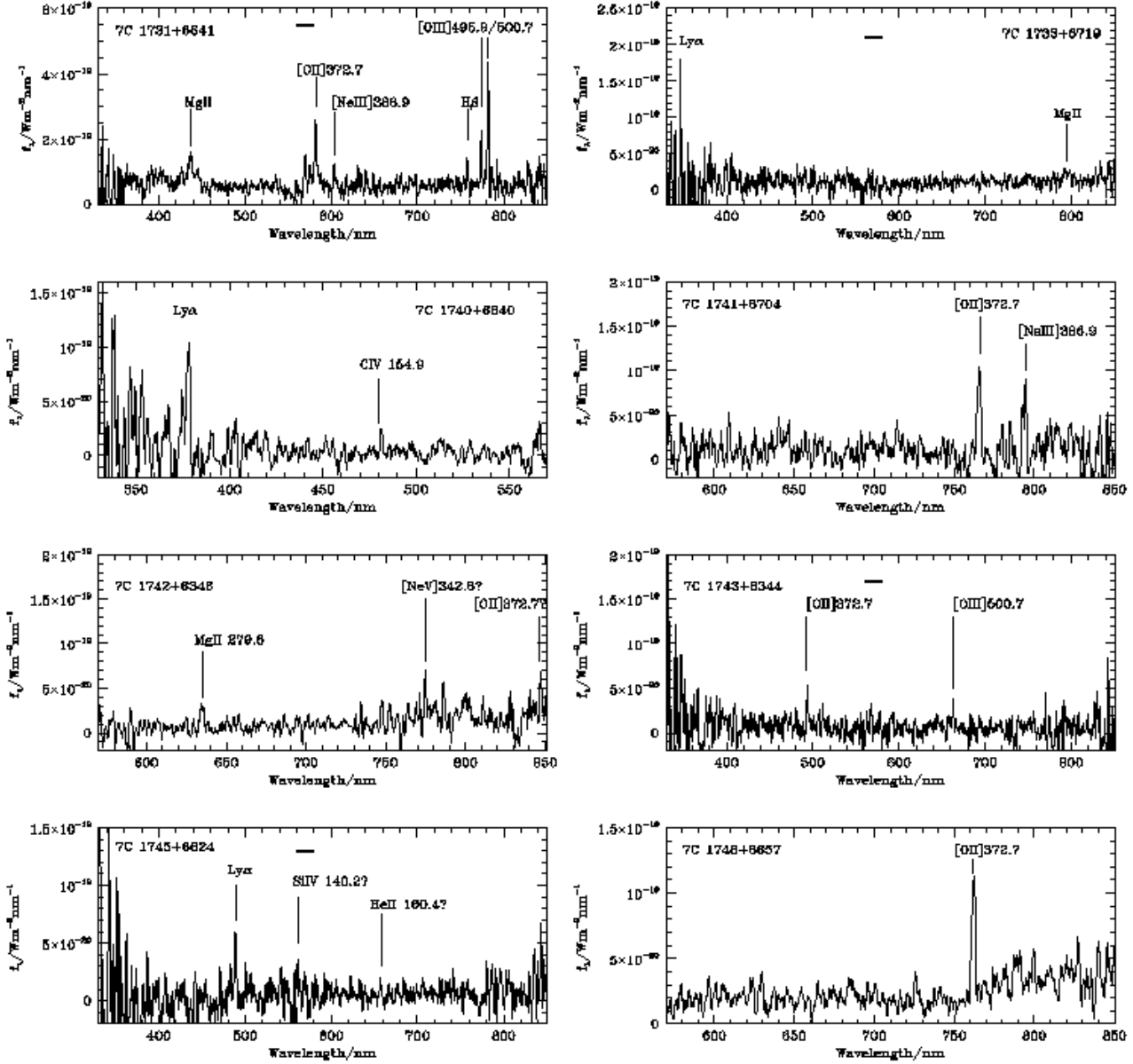


Figure 1. Spectra of objects in the 7C-III sample. The thick black bars on some of the plots show the wavelength region where the dichroic transmission was $\ll 1$ on the crossover from the red to blue arms. This region is noisy and sensitive to inaccuracies in the calibration.

Another possible source of bias is the existence of objects with anomalously low Ly α emission (e.g. van Ojik et al. 1994, Dey et al. 1995). So far, all examples of these have fairly strong high ionisation lines, but this may simply be a selection effect, as objects without these would be very hard to obtain redshifts for. If Ly α extinction is common, then many of the objects without redshifts and without continuum emission in the blue arm could be very distant.

Finally, it has recently become apparent that many of the highest redshift radio sources are amplified by gravitational lensing effects. For example two well-studied $z > 4$

radio galaxies have foreground galaxies within a few arcseconds of the line of sight (Lacy et al. 1994; Rawlings et al. 1996), and significant overdensities of foreground galaxies have been found in the fields of high redshift 3C radio sources (Benítez et al. 1997). Misidentification of the radio galaxy with a lensing object could lead to a substantial underestimate of the radio source redshift. Accurate astrometry is the best safeguard against this, but also lensing galaxies are unlikely to have the high equivalent width emission lines frequently found in radio galaxies. We therefore feel that this is probably not important for our sample, where

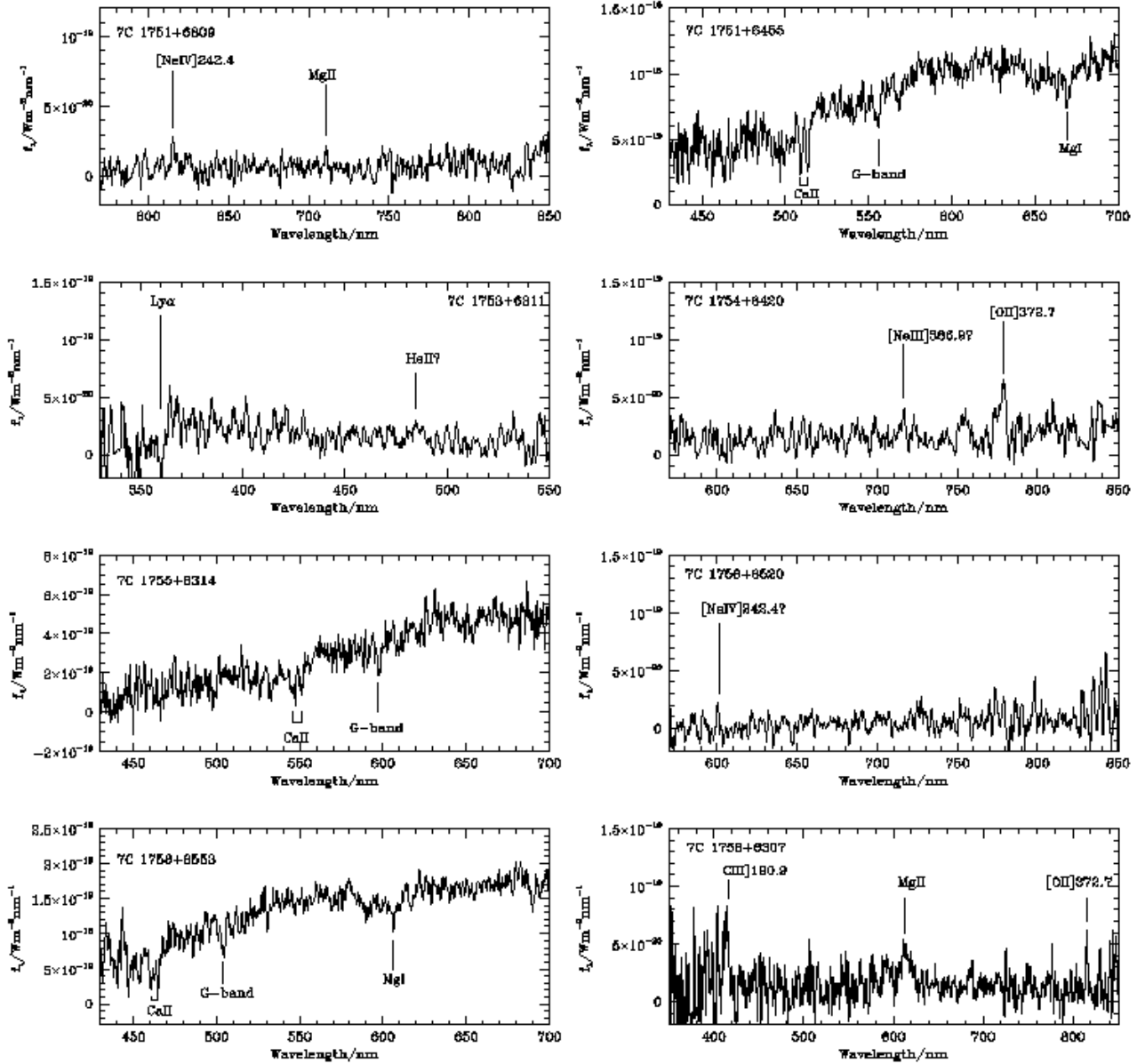


Figure 1. continued

nearly all the $z > 1$ objects with established redshifts have spectra characteristic of active galaxies. We note, however, several cases in which a low redshift galaxy lies close enough to the radio structures to be mistaken for the identification, but which we found through imaging or spectroscopy were foreground objects. Some probable lensing events are discussed in Section 7.

4.3 Notes on individual objects

7C 1740+6640

This radio galaxy was observed in R -band through the Auxiliary Port of the WHT on 1995 July 30 (Fig. 4). The airmass was 1.8, and the seeing 0.8-arcsec. The identification has $R = 24.8$ in a 3-arcsec diameter aperture.

The Ly α line seen in the spectrum of this object appears to have a weak blueshifted component at $z = 2.081$, compared to $z = 2.109$ for the main Ly α component.

Table 4. Results of spectroscopy of the 7C-III radio sources

Name	Redshift	Grade	Emission line	Flux / 10^{-20}Wm^{-2}	Width / kms^{-1}	Equivalent width/nm	Comments
7C 1731+6641	0.561	α	MgII279.8	100	10500	19.2	broad component
			[OII]372.7	50	-	4.9	
			[NeIII]386.9	26	-	-	
			H β	17	-	2.8	
			[OIII]495.9	30	-	4.9	
			[OIII]500.7	68	-	11.2	
7C 1732+6535*	0.856	$\alpha?$					Literature z (Paper II)
7C 1733+6719*	1.84	β	Ly α	22	-	-	
			MgII279.8	164	3000	16.1	broad component
7C 1736+6710*	0.188	α					Paper II
7C 1740+6640	2.10	α	Ly α	41	-	-	double
			CIV154.9	3	-	-	
7C 1741+6704*	1.054	α	[OII]372.7	29	-	-	
			[NeIII]386.9	22	-	-	
7C 1742+6346*	1.27	β	MgII279.8	10	-	-	
			[NeV]342.6	8	-	-	uncertain
			[OII]372.7	8	-	-	uncertain
7C 1743+6344*	0.324	α	[OII]372.7	8	-	-	ID uncertain, see notes
			[NeIII]386.9	4	-	-	
			[OIII]500.7	5	-	-	
7C 1743+6431*	?	-					no lines
7C 1743+6639*	0.272	α					Paper II
7C 1745+6415*	0.673	α	[OII]372.7	80	-	280	LRWLR
			H β	40		63	
			[OIII]495.9	140		170	
			[OIII]500.7	400		460	
7C 1745+6422*	1.23	α					K95
7C 1745+6624	3.01	β	Ly α	17			
			SiIV 140.2	5			uncertain
			HeII 164.0	3			uncertain
7C 1747+6533*	1.516	α					K95
7C 1748+6703*	?	-					see notes
7C 1748+6657*	1.045	β	[OII]372.7	26	-	17	plus continuum break
7C 1748+6731*	0.56	α	[OIII]500.7?	9	-	1	LRWLR
7C 1751+6809*	1.54	β	[NeIV]242.4	4	-	-	
			MgII 279.8	2	-	-	
7C 1751+6455*	0.294	α					absorption line z
7C 1753+6311*	1.96	γ	HeII	7	-	-	+Ly α absorption?
7C 1753+6543*	0.140	α					R.G. McMahon (p.c.)
7C 1754+6420*	1.09	β	[OII]372.7	19	-	-	diffuse
			[NeV]342.6	7	-	-	
7C 1755+6314*	0.388	α					absorption line z
7C 1755+6830*	0.744	α	[OII]372.7	20	-	2.4	LRWLR
			[NeIII]386.9	17	-	-	
			[NeV]342.6?	20	-	-	
7C 1756+6520*	1.48	γ	[NeIV]242.4?	4			see notes
7C 1758+6535*	0.80	α	[OII]372.7	18		14	LRWLR
			[NeIII]386.9	10	-	-	
7C 1758+6553*	0.171	α					absorption line z
7C 1758+6307*	1.19	α	CIII]190.9	45	5100	-	
			MgII 279.8	41	6600	31	
			[OII]372.7	12	-	17	
7C 1758+6719*	2.70	α	Ly α (north)	120	-	-	double
			Ly α (south)?	30	-	-	-38000 kms^{-1}
			CIII]190.9	8	-	-	from north component.

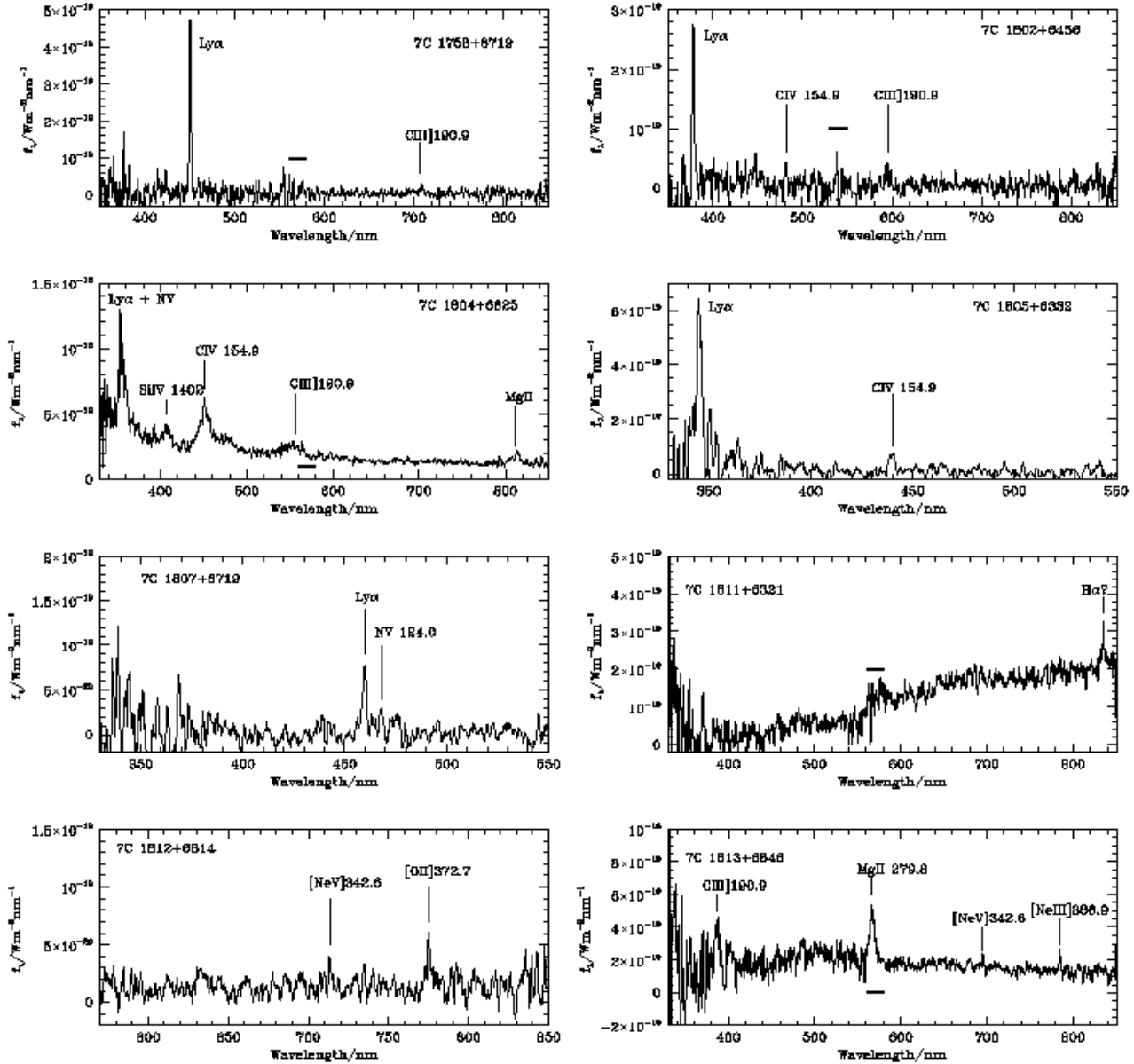


Figure 1. continued.

7C 1742+6346

The redshift of this object is uncertain as both the [NeV] and [OII] emission line candidates are in regions of high sky noise, so may not be real. No emission was detected from the region of the putative central component. A number of other objects were present along the slit (see image in Paper III). Galaxy ‘a’ has emission lines at $z = 0.326$, and may be a member of the nearby cluster A2280 whose cD galaxy is 4.5 arcmin distant and has $z = 0.330$ (Paper II). Galaxy ‘b’ has a single emission line consistent with [OII]372.7 at $z = 0.457$.

7C 1743+6344

The identification of this object in Paper II is about 4-arcsec due north of the mid-point of the radio hotspots. In our spectrum emission lines at $z = 0.324$ and very faint continuum are seen close to the mid-point of the radio hotspots, and the original candidate identification also appears to have [OII] emission at the same redshift. Whichever of these two objects is the correct identification, this radio source is very unusual in having such an apparently subluminal optical counterpart. The redshift is consistent with the radio source being a member of the A2280 cluster, whose cD galaxy is nearby (Paper II).

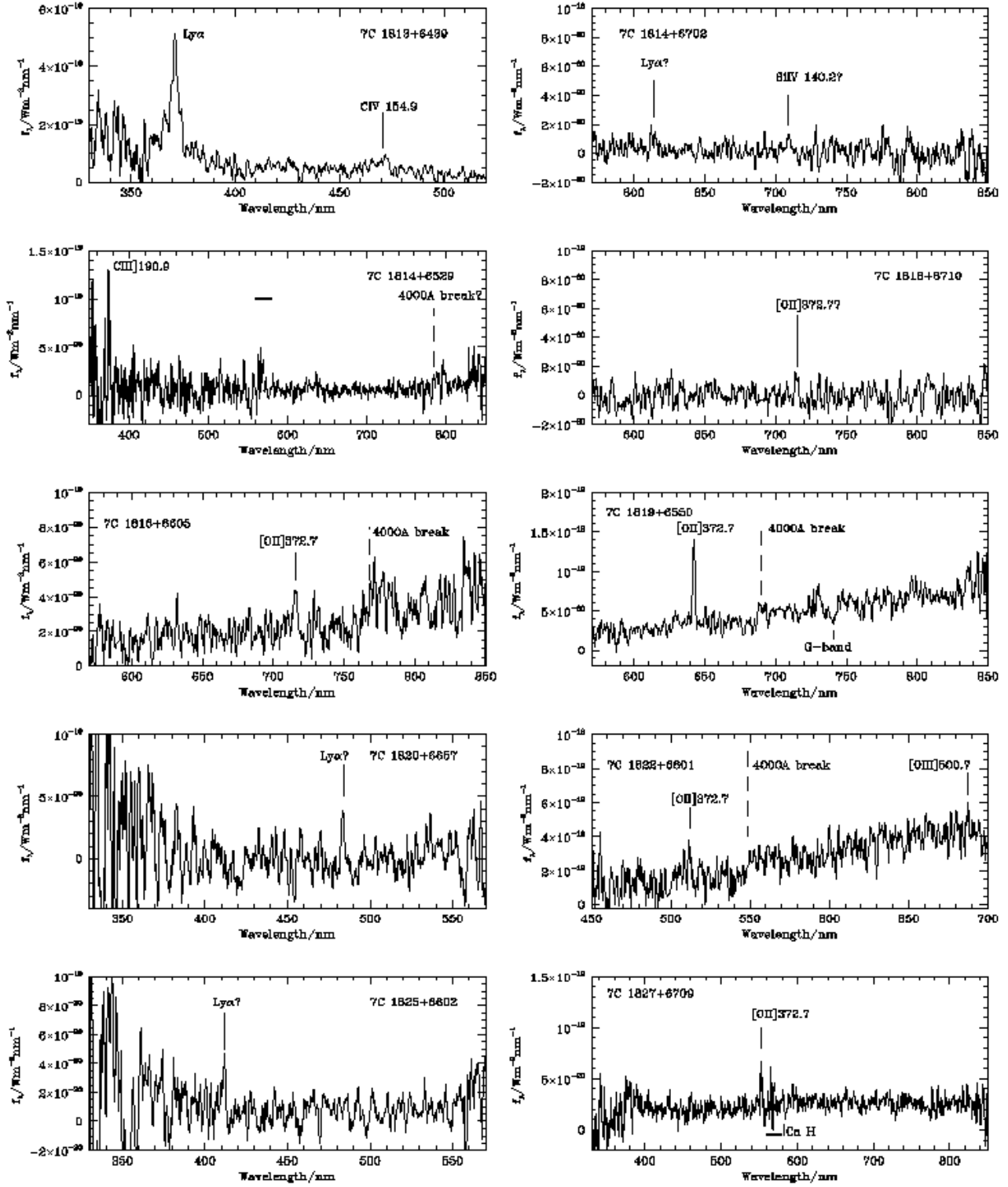


Figure 1. continued.

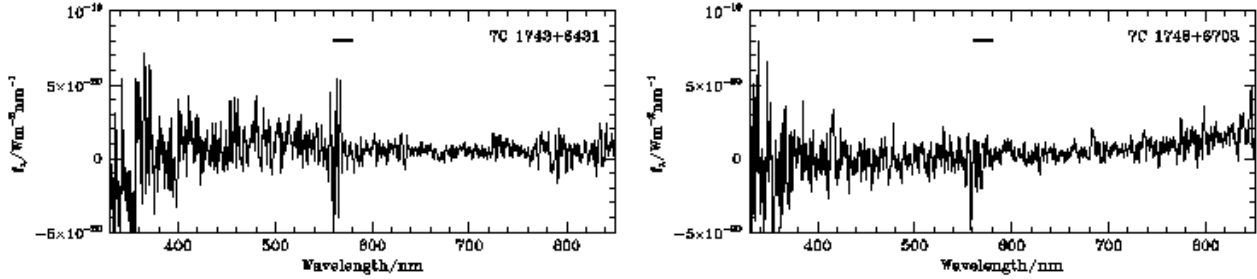


Figure 2. Featureless spectra, displayed as in Fig. 1

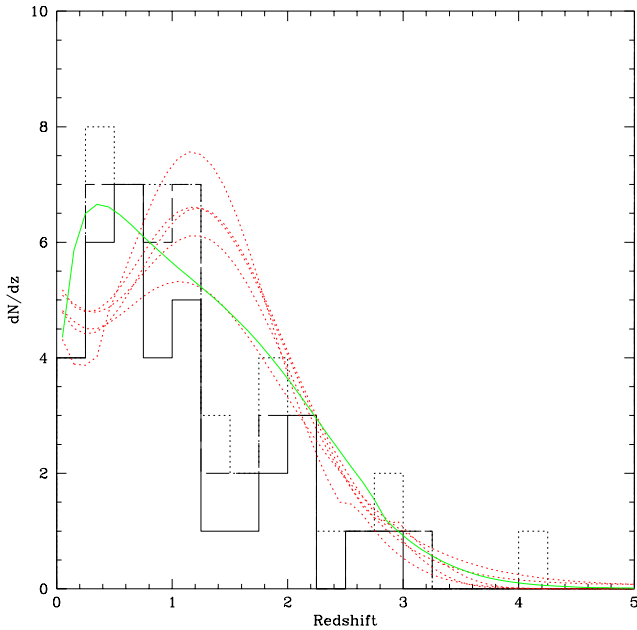


Figure 3. Redshift distribution of the 7C-III sample. The distribution of grade α redshifts is shown as the solid histogram. β redshifts are added in as dot-dash lines and γ redshifts as dotted lines. The curves are the predictions of the Dunlop & Peacock (1990) models: the dotted lines are the free-form models and the solid line the luminosity-density evolution model.

7C 1743+6431

The original identification of this radio source in Paper II is probably incorrect. As discussed in Paper III, an object on the H -band image is coincident with the position of a tentative radio central component in Paper I. The H -band object is very faint in the optical and no emission lines are discernible in the WHT spectrum, although the detection of continuum down to 447nm allows us to constrain the redshift to < 3.9 . The photometric redshift obtained assuming $H - K = 1$ and the $K - z$ relation of Eales et al. (1997) is ≈ 1.7 , consistent with no strong lines being seen in the spectrum and the very red $R - K$ colour. The original identification has a redshift of 0.364, and is close to the western hotspot. It may therefore be magnifying the hotspot through gravitational lensing effects.

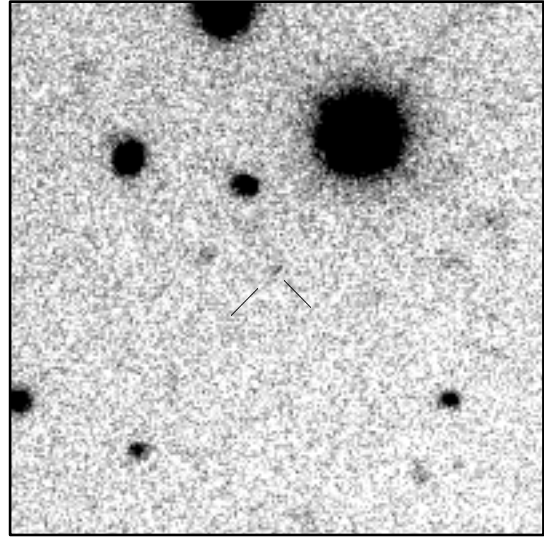


Figure 4. R -band image of 7C1740+6640. The image is 20 arcsec square, and the position of the identification is marked. North is to the top and east to the left.

7C 1745+6624

This object was also observed on the NASA Infrared Telescope Facility (IRTF) on 1998 February 15 for 30 min through the K' filter (Fig. 5). The airmass was 1.7. An object is just detected at the $3 - \sigma$ level 0.6 arcsec E and 1.1 arcsec south of the position of the radio point source, with $K \approx 20.8$ in a 2-arcsec diameter aperture.

Although only the $\text{Ly}\alpha$ line is strongly detected in the spectrum, the faint K' magnitude is consistent with the relatively high redshift of 3.01, as are marginal detections of $\text{SiIV } 140.2$ (unfortunately in the dichroic region) and $\text{HeII } 164.0$, along with a possible continuum break across $\text{L}\alpha$.

7C 1748+6703

No emission is seen from a spectrum centred on the radio position of the assumed radio central component. In Paper III we discuss the detection of a galaxy ≈ 2 arcsec north of this position, in addition to a very faint object coincident with the radio central component. The galaxy ≈ 10 arcsec east of the radio position has an emission line at 683.5 nm and a red continuum. If the emission line is $[\text{OII}]$ the redshift of this galaxy is 0.83. Both this galaxy and the galaxy to the

Table 4. Results of spectroscopy of the 7C-III radio sources continued

Name	Redshift	Grade	Emission line	Flux / $10^{-20} \text{ W m}^{-2}$	Width /kms $^{-1}$	Equivalent width/nm	Comments
7C 1801+6902*	1.27	α					Paper II
7C 1802+6456*	2.11	α	Ly α	71	-	48	
			Civ 154.9	10	-	-	
			Ciii]190.9	8	-	-	
7C 1804+6625	1.91	α	Ly α	270	3000	5	
			Nv 124.0	110	3700	2	
			Siv 140.2	120	8000	5	
			Civ 154.9	470	11000	20	
			HeII 164.0	160	11000	7	width fixed to Civ
			MgII 279.8	90	4500	8	
7C 1804+6313*	?	-					missed
7C 1805+6332*	1.84	α	Ly α	170	1800		see notes
			Civ 154.9	25	1800		
7C 1807+6831*	0.58	α	[OII]372.7	11	-	-	LRWLR
			[NeIII]386.9	8	-	-	
			[OIII]500.7	22	-	-	
7C 1807+6719*	2.78	α	Ly α	21	-	-	
			Nv 124.0	7	-	-	
7C 1807+6841*	0.816	α	[OII]372.7	52	870	21	LRWLR
			[NeIII]386.9	11	580	4	
7C 1811+6321*	0.273	γ	H α ?	15	-	-	
7C 1812+6814	1.08	α	[NeV]342.6	5	-	-	
			[OII]372.7	10	-	-	
7C 1813+6846*	1.03	α	Ciii]190.9	150	-	10	
			MgII 279.8	170	3000	7	
			[NeV]342.6	10	-	0.6	
			[NeIII]386.9	26	-	2	
7C 1813+6439*	2.04	α	Ly α	4100	200	20	
			Civ 154.9	6700	49	135	
7C 1814+6702*	4.05	γ	Ly α	5	-	-	see notes
			Siv 140.2	3	-	-	
7C 1814+6529*	0.96	β	Ciii]190.9	31	-	-	plus 4000Å break
7C 1815+6805*	0.230	α	-	-	-	-	Paper II; K95
7C 1815+6815*	0.794	α	MgII 279.8	20	-	-	plus 4000Å break; LRWLR
7C 1816+6710*	0.92	γ	[OII]372.7	4	-	-	see notes
7C 1816+6605*	0.92	β	[OII]372.7	6	-	3	plus 4000Å break
7C 1819+6550*	0.724	α	[OII]372.7	20	-	6	plus 4000Å break
7C 1820+6657	2.98	γ	Ly α ?	10	-	-	
7C 1822+6601*	0.37	α	[OII]372.7	40	-	2.4	
			[OIII]500.7	12	-	0.3	
7C 1825+6602*	2.38	γ	Ly α ?	7	-	-	see notes
7C 1826+6510*	0.646	α	-	-	-	-	LRWLR
7C 1826+6704*	0.287	α	-	-	-	-	Paper II
7C 1827+6709*	0.48	β	[OII]372.7	10	-	5	plus Ca H (Ca K lost in sky line)

Notes: Linewidths are only given for emission lines significantly broader than the instrumental width ($\approx 1500 \text{ kms}^{-1}$ at 500 nm for the WHT data). Equivalent widths are only given where the continuum is detected at high signal:noise. Asterisks by the names indicate members of the NEC* sample defined in Section 9. The redshift grades are α for a firm redshift, β for a less certain redshift and γ for an uncertain one, as discussed in Section 4.1. A dash indicates that no redshift could be measured.

north are probably close enough to the radio source to be magnifying it via gravitational lensing if the redshift of the radio galaxy is $\gg 1$.

7C 1753+6311

This object has a very unusual spectrum, with very blue continuum colours (approximately flat in f_ν), but no strong

emission lines. We have tentatively identified an apparent break in the UV spectrum with Ly α absorption at $z = 1.96$, also consistent with a weak emission feature at 485 nm being HeII 164.0. The apparent break may, however, be due to a combination of the atmospheric cutoff and low signal-to-noise, so the redshift must be considered tentative until a better spectrum can be obtained. The EW of the UV emission lines must be fairly low for us not to have detected any. Indeed the spectrum is much more reminiscent of starburst

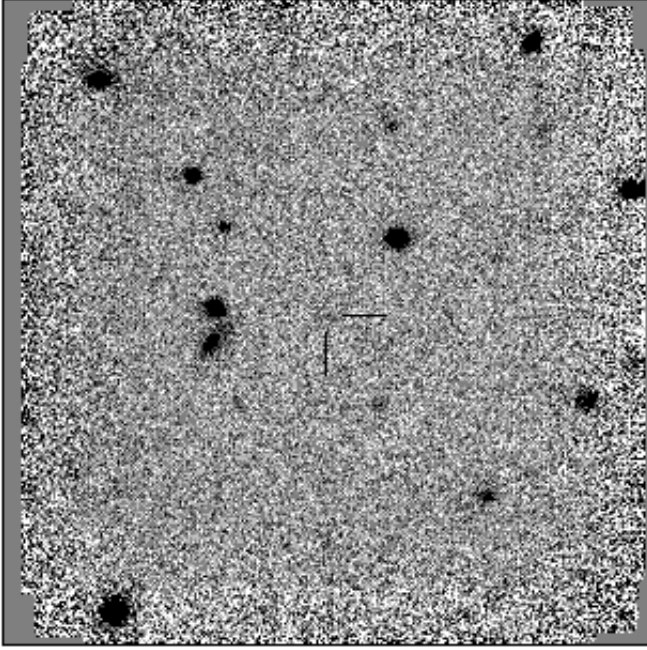


Figure 5. K' image of 7C1745+6624. The image is 93 arcsec square, and the position of the identification is marked. North is to the top and east to the left.

galaxies than of AGN, suggesting a starburst may be the origin of the blue light; in this case the AGN must be either very weak compared to some of our other $z \sim 2$ radio galaxies or obscured by the starburst. This source also has an unusual radio structure (Paper I).

7C 1756+6520

The spectrum of this object shows very faint ($R \approx 24$) continuum throughout the spectrum which is approximately constant in f_λ . There is a marginally-significant emission line at 600.5 nm. It is unlikely to be $\text{Ly}\alpha$ due to the lack of any continuum drop shortward of the emission line wavelength, and in particular the presence of flux below the redshifted Lyman limit at 450 nm. On the other hand, the faintness of the continuum emission suggests a higher redshift than the 0.6 derived from assuming the line is $[\text{OII}]372.7$. We have therefore assigned a very tentative redshift of 1.48 to this object, assuming that the emission line is $[\text{NIV}]242.4$, one of the brightest lines for which we would not expect to see bright $\text{Ly}\alpha$ or $[\text{OII}]372.7$ emission in the spectrum. In the composite spectrum of McCarthy (1994), this and $\text{CII}]232.6$ are comparably bright, but if we assume the line is $[\text{NIV}]$ then the $\text{CII}]$ line would be in the dichroic region and therefore quite likely to have been missed.

7C 1758+6719

This object was originally identified with a faint optical object approximately midway between two radio components, which are 45 arcsec apart (Paper II). We placed our slit through both radio components and the optical object. $\text{Ly}\alpha$ and CIV emission were seen from the northern component at $z = 2.70$. We also found a single emission line from the approximate position of the southern radio component at 395.2

nm, which, if $\text{Ly}\alpha$, would correspond to a redshift of 2.25. The original identification has a single emission line at 665.3 nm, with a possible second line at 776.4 nm in the sky lines, which could correspond to $[\text{OII}]372.7$ and $\text{H}\gamma$ at $z = 0.785$. HST, MERLIN and VLA imaging and together with further optical spectroscopy of this enigmatic radio source will be presented in a future paper.

7C 1802+6456

A galaxy with strong emission lines at $z = 0.69$ is seen within 2-arcsec of the western hotspot. It is probably magnifying the hotspot emission via gravitational lensing.

7C1804+6313

This object has no clear identification. A marginally-resolved radio component was discovered in Paper I, but subsequent VLA mapping presented in Paper III showed that this was just one end of a low surface brightness radio galaxy. A spectrum was taken through objects 'a', 'b' and 'F' of Paper III, and a further one through 'a' alone; all these objects seem to be stars. The most likely identification is therefore probably object 'c' of Paper III for which we have yet to obtain a spectrum.

7C 1805+6332

The original identification of this object in Paper II was an $R = 21.1$ galaxy 3 arcsec from the line joining the midpoint of the radio hotspots. The spectroscopic observations were made with the slit placed so as to cover both the proposed identification and the midpoint of the hotspots. The resulting spectrum shows that the true identification lies close to the midpoint of the hotspots, with the original identification being foreground, with a probable redshift (based on $\text{H}\alpha$ in emission and MgI in absorption) of 0.32. This is another example of an object which may be being amplified by gravitational lensing.

7C 1811+6321

This object has a largely featureless red continuum, apart from one strong emission line which is taken to be $\text{H}\alpha$. The nearby, unaligned companion galaxy has no spectral features, but has a similar spectral energy distribution to the radio galaxy.

7C 1814+6702

This object shows very faint continuum between 615 and 700 nm. There are two very marginally-detected emission line candidates whose ratio of wavelengths is consistent with $\text{Ly}\alpha:\text{SiIV } 140.2$ at $z = 4.05$ or $[\text{NIV}]242.4:\text{MgII}$ at $z = 1.53$. As there is no sign of continuum emission shortward of the shortest wavelength emission line candidate we have provisionally taken the redshift to be $z = 4.05$ pending further spectroscopy, although this should probably be considered an upper limit on the true value of the redshift.

Table 7. Candidate gravitationally-lensed radio galaxies

Name	z_{Source}	z_{Lens}	Notes
8C1742+637	1.27	0.33?	Weak lensing of both hotspots?
8C1743+645	$\sim 1.7?$	0.36	Probable lensing of W hotspot
8C1802+649	2.11	0.69	Probable lensing of W hotspot
8C1805+635	1.84	0.32	Lobe is probably lensed

7C 1816+6710

This object shows only a single faint, spatially extended emission line and faint continuum. We assume the line is [OII] as there is no sign of a drop in the continuum shortward of the line wavelength.

7C 1825+6602

Another object showing only a single, marginally-detected faint emission line and faint continuum. The continuum emission is approximately constant in f_λ throughout both arms of the spectrum. We have assumed the single emission line detected in the blue to be $\text{Ly}\alpha$ at $z = 2.38$, but it is also possible that this object lies in the $z = 1.3 - 1.8$ range where there are no strong emission lines. The apparent blue continuum excess shortward of our assumed $\text{Ly}\alpha$ line is probably light refracted into the slit from a nearby star.

5 GRAVITATIONAL LENSING

A number of coincidences of foreground galaxies and clusters with 7C-III and 8C-NEC sources have been noted in both this paper and Paper III. The best candidates for lensing are listed in Table 7, along with source and lens redshifts where known. There may also be others which will only become apparent once deeper images or spectra are obtained. High redshift radio sources present a large geometrical cross-section to lensing, particularly when selected at low frequency where the extended heads and lobes can still contribute significantly to the total flux. Because of this large size, however, magnification factors are typically modest, $\lesssim 2$ and the effect on the luminosity function may be fairly unimportant, at least at $z \lesssim 4$ (Lacy 1998). Follow-up observations of these objects, together with the lensing statistics of the samples and their implications will be discussed in a future paper.

Studies of larger samples of high redshift radio sources should allow us to investigate the effect of lensing on the observed radio luminosity function at high redshift. We will also be able to make determinations of mass:light ratios for significant numbers of lensing galaxies in the range $0.3 \lesssim z \lesssim 1$.

6 COSMIC EVOLUTION OF THE RADIO SOURCE POPULATION

As we have complete samples at both 38 and 151 MHz we are able to introduce an important refinement to the study of the cosmic evolution of radio sources. All previous studies have been limited to samples selected at a particular observed frequency, which corresponds to different rest-frame frequencies depending on the redshift of the radio source.

Table 8. Surveys used to determine flux densities in the NEC

Frequency	Beamsize	Reference
38 MHz	$4.5 \times 4.5 \text{ cosec } \delta \text{ arcmin}^2$	Rees 1990
151 MHz	$70 \times 70 \text{ cosec } \delta \text{ arcsec}^2$	Lacy et al. 1995
327 MHz	$54 \times 54 \text{ cosec } \delta \text{ arcsec}^2$	Rengelink et al. 1997
408 MHz	$3.4 \times 3.4 \text{ cosec } \delta \text{ arcmin}^2$	Roger, priv. comm.
1.5 GHz	$\approx 20 \times 20 \text{ arcsec}^2$	Kollgaard et al. 1994
2.695 GHz	$4.5 \times 4.5 \text{ arcmin}^2$	Loiseau et al. 1988
5 GHz	variable	Paper I or Greenbank

Note: Greenbank fluxes are from Gregory & Condon (1991), or Becker, White & Edwards (1991).

Thus a sample selected at, say, an observed frequency of 151 MHz is effectively selecting $z = 2$ sources at 453 MHz. Furthermore, all such samples are selected on the basis of flux density (S_ν) rather than emitted flux.

Investigating the importance of this effect is hard, particularly at low radio frequencies as the K -corrections are uncertain and usually have to rely on an extrapolation of the spectrum measured at high frequencies. In the NEC, we have the 38MHz fluxes to supply the low frequency point for the 151MHz 7C-III sample, and a variety of deep, higher frequency radio surveys to derive an accurate radio source spectrum from. The surveys used are listed in Table 8. Note that the comparable or higher angular resolution offered by many of these surveys means that confusion of source fluxes can be practically eliminated. Copies of the Table containing the flux information for the sources listed in this paper will be made available over the Internet (www-astro.physics.ox.ac.uk/~mdl).

6.1 Selection of a new complete sample

We have elected to select our sample based on νS_ν in the rest-frame of the radio source. If we select with a flux limit of $(\nu_s S_{\nu_s})_{\text{Limit}}$ at a selection frequency ν_s in the rest-frame of the radio source, this is equivalent to a limit of

$$\frac{\nu_s}{(1+z)} S_{[\nu_s/(1+z)]} \geq (\nu_s S_{\nu_s})_{\text{Limit}}$$

in the observed frame. We work out $S_{[\nu_s/(1+z)]}$ using a fit to the radio spectrum described below. Cancelling out ν_s our selection then reduces to imposing a redshift-dependent flux density limit:

$$\frac{S_{[\nu_s/(1+z)]}}{1+z} \geq (S_{\nu_s})_{\text{Limit}}.$$

We argue that this is a more physically useful way of defining a sample as the selection is based directly on power emitted at low frequency rather than on flux received per unit frequency. There are of course many alternative selection methods one could think of (for example integrating the spectrum in the rest frame over some larger frequency range), but this criterion has the advantage of being simple to implement. For the NEC samples we have used a selection criterion of $S_{151(\text{rest})}/(1+z) \geq 0.45 \text{ Jy}$, obtaining $S_{151(\text{rest})}$ from fitting quadratics in log frequency versus log flux density to obtain smooth spectra in the range 38 - 4850 MHz. The flux density limit of the 8C-NEC sample is $S_{38} = 1.3 \text{ Jy}$ in the observed frame, comfortably below the limit for a $z \approx 3$ source from the 7C-III sample which has its rest-frame

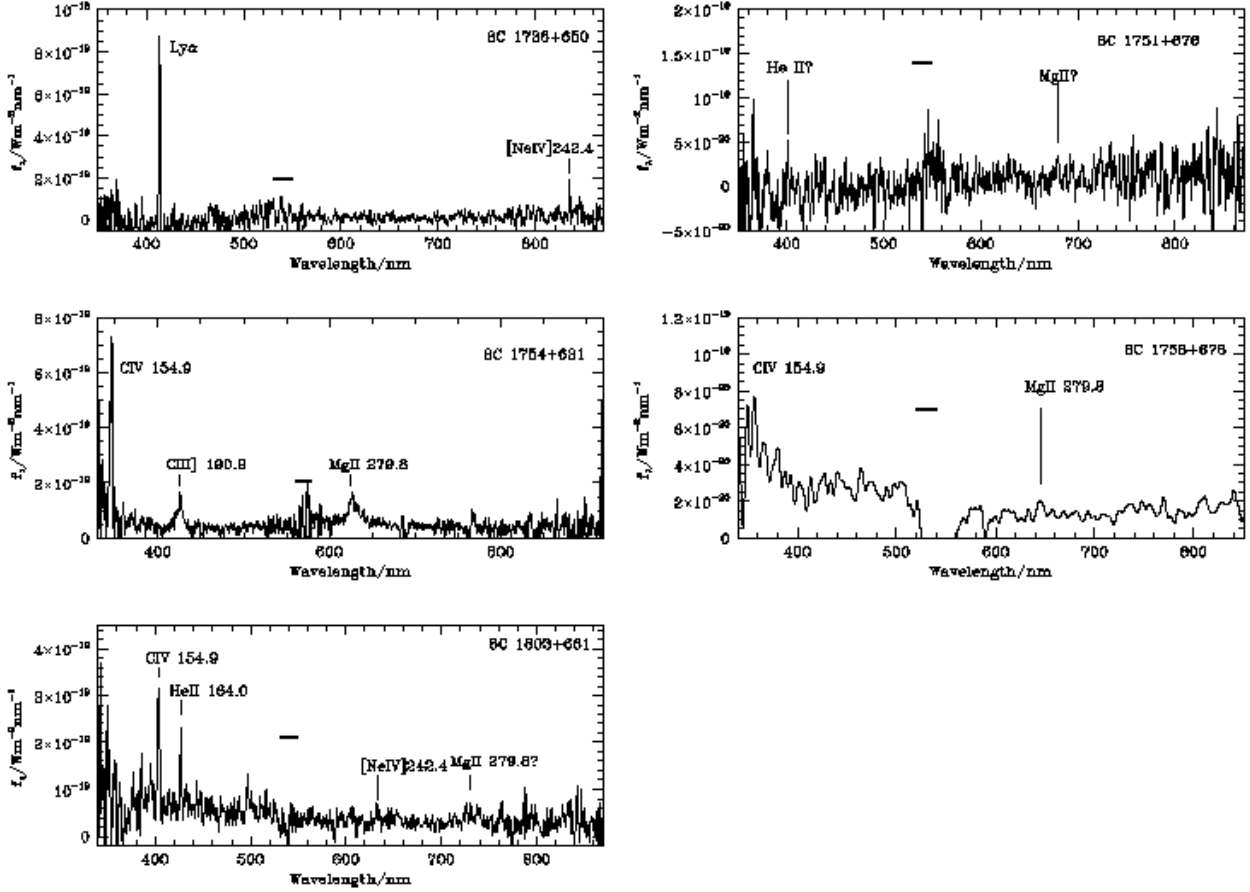


Figure 6. Spectra of 8C-NEC objects not in the 7C-III sample

Table 5. Log of new spectroscopy of the 8C-NEC radio sources

8C Name	Observing date(s)	Telescope	wavelength range(s)	integration time(s)/sec	slit width /arcseconds	slit PA	airmass
8C 1736+650	19/06/93	WHT	330 - 850 nm	1200	3	70	1.25
8C 1751+676	19/06/93	WHT	330 - 850 nm	3600	2	18	1.29
8C 1754+631	20/08/93	WHT	330 - 900 nm	1800	3	90	1.60
8C 1758+676	04/07/97	Shane	330 - 1060 nm	3600	2	50	1.3
8C 1803+661	17/06/93	WHT	330 - 850 nm	1200	3	122	1.26

151-MHz flux emitted at 38 MHz, namely $S_{38} = 2\text{Jy}$. Objects which are bright enough to meet the selection criteria for this sample, which we shall refer to as the NEC* sample, are marked with an asterisk in Tables 4 and 6. Rest-frame 151-MHz flux densities and 1-GHz spectral indices are given in Table A2 of the Appendix.

For sources without redshifts, if they lie above the flux limits of the sample in the observed frame, 0.5 Jy at 151 MHz and 2Jy at 38 MHz, they are counted as being in the NEC* sample, and conversely if they lie below both flux limits they are not. This test is ambiguous for only one object, 8C 1808+677. This object has $S_{38} = 2.0\text{ Jy}$ and will therefore

only be included if it is at $z \geq 3$; we therefore have excluded this object from the sample.

The resulting sample contains 51 objects, 33 of which have α redshifts, eight β redshifts, seven γ redshifts and three objects with no redshift information.

The primary effect of the νS_ν selection is to remove the compact steep spectrum (CSS), objects from the 7C-III sample. These drop out as they often have spectra which

Table 6. Results of spectroscopy of the 8C-NEC radio sources

8C Name	7C Name (if in 7C-III sample)	z	Grade	Emission line	Flux / 10^{-20}Wm^{-2}	Width /kms $^{-1}$	Equivalent width/nm	Comments
8C 1732+655*	7C 1732+6535	0.856	$\alpha?$					Paper II
8C 1733+673*	7C 1733+6719	1.84	β			-	-	new member (L98)
8C 1736+650*	-	2.40	α	Ly α	180	-	-	
				[NeIV]242.4	23	-	-	
8C 1736+670*	7C 1736+6710	0.188	α					Paper II
8C 1741+670*	7C 1741+6704	1.054	α			-	-	
8C 1742+637*	7C 1742+6346	1.27	β			-	-	
8C 1743+637*	7C 1743+6344	0.324	α			-	-	ID uncertain,
8C 1743+645*	7C 1743+6431	?	-			-	-	
8C 1743+666*	7C 1743+6639	0.272	α					Paper II
8C 1745+642*	7C 1745+6415	0.673	α			-		
8C 1745+644*	7C 1745+6422	1.23	α					K95
8C 1747+655*	7C 1747+6533	1.516	α					K95
8C 1748+670*	7C 1748+6703	?	-					see notes
8C 1748+675*	7C 1748+6731	0.56	α					
8C 1751+681A*	7C 1751+6809	1.54	β			-	-	
8C 1751+681C	-	?						no spectrum
8C 1751+676*	-	1.42	γ	HeII164.0?	8			
				MgII279.8?	9			
8C 1751+649*	7C 1751+6455	0.294	α					
8C 1753+631*	7C 1753+6311	1.96	β			-	-	
8C 1753+664	-	?						no spectrum
8C 1753+657*	7C 1753+6543	0.140	α					
8C 1754+643*	7C 1754+6420	1.09	β			-	-	
8C 1754+631	-	1.23	α	CIV 154.9	220	3000	25	
				CIII]190.9	86	6100	24	
				MgII 279.8	130	7300	21	
8C 1755+632*	7C 1755+6314	0.388	α					
8C 1755+685B*	7C 1755+6830	0.744	α					
8C 1757+653*	7C 1756+6520	1.48	γ					
8C 1758+676	-	1.31	β	CIV 154.9	55	-	18	
				MgII279.8	6	-	5	
8C 1758+655*	7C 1758+6535	0.80	α					
8C 1758+658*	7C 1758+6553	0.171	α					
8C 1758+631*	7C 1758+6307	1.19	α					
8C 1758+673*	7C 1758+6719	2.70	α			-	-	

are flattening towards low frequency. They are replaced with extended, steep spectrum objects [†].

The redshift distributions of the NEC*, 8C-NEC and 7C-III samples are compared in Fig. 7. As can be seen there are no strong dependencies of the redshift distribution on the sample selection method. The largest change is seen at

[†] Absorption of low frequency emission in our Galaxy is unlikely to be causing objects to drop out through spectral flattening at low frequency. Kassim (1989) finds that supernova remnants at galactic latitudes $|b| \gtrsim 3^\circ$ have no evidence for low frequency turnovers at 30.9 MHz, although these are common for remnants closer to the plane and seen towards the inner galaxy. For comparison the NEC is at galactic coordinates $l^{\text{II}} = 96^\circ$, $b^{\text{II}} = +30^\circ$, so on that basis galactic absorption is unlikely to be significant. Perhaps the best argument against galactic absorption, however, is that the objects which do show spectral flattening at low frequencies tend to be CSS sources, where there are plausible physical reasons for an intrinsic turnover in the source spectrum.

$z > 2$, where three of the 7C-III high- z CSS sources drop out of both the NEC* and the 8C-NEC samples, and one extended $z > 2$ object (8C1736+650) comes in to both the NEC* and 8C-NEC samples.

For comparison with high radio luminosity objects we have used similar selection criteria to define a bright sample (3C*). This is described in the Appendix.

6.2 A complete listing of the samples

In this subsection we present a complete listing of the 8C-NEC, 7C-III and NEC* samples in a single table for ease of reference. Object classifications into low-excitation narrow-line radio galaxy (LEG), high-excitation narrow-line radio galaxy (HEG), weak quasar (WQ) and quasar (Q) follow a combination of Jackson & Rawlings (1997) and Willott et al. (1998) criteria. For galaxies with [OIII]500.7 in the optical band ($z < 0.7$ for most spectra) we have split the radio

Table 6. Results of spectroscopy of the 8C radio sources continued

8C Name	7C Name (if in 7C-III sample)	z	Grade	Emission line	Flux / 10^{-20}Wm^{-2}	Width /kms $^{-1}$	Equivalent width/nm	Comments
8C 1801+690*	7C 1801+6902	1.27	α					
8C 1802+649*	7C 1802+6456	2.11	α					
8C 1803+661*	-	1.61	α	CIV 154.9	53	-	6	
				HeII 164.0	26	-	4	
				CIII]190.9	19	-	3	
				[NeIV]242.4	5	-	1	
				MgII 289.8?	49	9000	19	broad?
8C 1804+664	7C 1804+6625	1.91	α					
8C 1804+632*	7C 1804+6313	?	-					
8C 1805+635*	7C 1805+6332	1.84	α					
8C 1807+685*	7C 1807+6831	0.58	α			-	-	
8C 1807+687*	7C 1807+6841	0.816	α					
8C 1808+677	-	?	-					no spectrum
8C 1811+633*	7C 1811+6321	0.273	γ					
8C 1813+687*	7C 1813+6846	1.03	α					
8C 1813+646*	7C 1813+6439	2.04	α					
8C 1814+670*	7C 1814+6702	0.95	γ					
8C 1814+657	-	0.95	β					Paper II
8C 1814+655*	7C 1814+6529	0.96	β					
8C 1815+680*	7C 1815+6805	0.230	α					
8C 1815+682*	7C 1815+6815	0.794	α					
8C 1816+671*	7C 1816+6710	0.92	γ					
8C 1816+660*	7C 1816+6605	0.92	β					
8C 1819+658*	7C 1819+6550	0.724	α					
8C 1821+643A*	-	0.298	α					
8C 1821+643B	-	0.304	$\alpha?$					Literature z
8C 1823+660*	7C 1822+6601	0.37	α					
8C 1826+660A*	7C 1825+6602	2.38	γ					
8C 1826+651*	7C 1826+6510	0.63	α					
8C 1826+670*	7C 1826+6704	0.287	α					
8C 1827+671*	7C 1827+6709	0.48	β					

Notes: Linewidths are only given for emission lines significantly broader than the instrumental width ($\approx 1500\text{ km s}^{-1}$ at 500 nm for the WHT data). Equivalent widths are only given where the continuum is detected at high signal:noise. Asterisks by the names indicate members of the NEC* sample defined in Section 9. The redshift grades are α for a firm redshift, β for a less certain redshift and γ for an uncertain one, as discussed in Section 4.1. A dash indicates that no redshift could be measured.

galaxies into LEG and HEG classes. LEGs are defined to have $[\text{OIII}]500.7\text{ EW} < 1\text{ nm}$ or $[\text{OII}]372.7/[\text{OIII}]500.7 < 1$, all other narrow-line radio galaxies are HEGs. Where $[\text{OIII}]$ is redshifted out of the optical band narrow-line radio galaxies are simply classified as NLG pending infrared spectroscopy. WQs have at least one broad line observed, but $M_B > -23$, whereas Qs have at least one broad line and $M_B < -23$ in unresolved flux. To calculate M_B we have assumed a power-law quasar spectrum with an optical spectral index of 0.5 for consistency with Willott et al. (1998).

7 CORRELATIONS OF FR II SOURCE PROPERTIES

A partial correlation analysis on the FR II or probable FR II sources from both the 7C-III + LRL and the NEC* + 3C* samples confirmed the same main dependences as those found for the 7C-I, II, 6C and 3C (LRL) samples studied by Blundell et al. (1999), namely that rest-frame spectral index at 1 GHz correlates best with radio luminosity, and that source size correlates best with redshift (also shown

in Paper II). Our trends are consistent with those seen by Blundell et al., although as our 3C sample is identical the results are not completely independent.

One difference between the 7C-III + LRL samples and the NEC* + 3C* samples is the lack of a strong spectral index – size correlation in the latter (Fig. 8). This seems to be being driven mostly by the flattening of the spectra of the CSS sources.

7.1 Size evolution

We show in Fig. 9 the redshift-size relation for FR II sources from the 7C-III+LRL and NEC*+3C* samples in two cosmologies. As is conventional we have parameterised the redshift dependence of source size in terms of the inverse scale factor $(1+z)$ as $D \propto (1+z)^{-\eta}$, and in Table 9 we give the best-fitting exponents η for all redshifts and, in the case of the NEC* + 3C* sample, for the grade α redshifts only. We have also tried adding the three objects without spectroscopic redshifts in, with all redshifts set to either 1.2 or 1.8, and find there is a small, but not significant reduction

Table 9. Complete listing of the samples

Object	Samples	z	grade	S_{38} /Jy	S_{151} /Jy	R	Size /kpc	Class	Notes
1731+6641	7C-III	0.561	α	0.9	0.52	21.4	7.4	HEG	
1732+6535	7C-III, 8C-NEC, NEC*	0.856	$\alpha?$	19.6	6.17	18.5	167	Q	
1732+6715	Temporarily excluded	-	-	6.1	0.88	-	-	-	Confused in radio
1733+6719	7C-III, 8C-NEC, NEC*	1.84	β	6.1	1.55	22.6	20.8	WQ	
1736+6504	8C-NEC, NEC*	2.40	α	2.2	0.48	23.0	133	NLG	
1736+6710	7C-III, 8C-NEC, NEC*	0.188	α	2.0	0.82	16.6	121	LEG	FRI
1740+6640	7C-III	2.10	α	0.9	0.54	24.8	<4.1	NLG	
1741+6704	7C-III, 8C-NEC, NEC*	1.054	α	1.9	0.72	22.8	33.4	NLG	
1742+6346	7C-III, 8C-NEC, NEC*	1.27	β	2.5	0.62	22.6	440	NLG	
1743+6431	7C-III, 8C-NEC, NEC*	?	-	8.2	1.89	23.3	-	?	
1743+6344	7C-III, 8C-NEC, NEC*	0.324	α	5.5	1.59	21.3	80.5	LEG	ID uncertain
1743+6639	7C-III, 8C-NEC, NEC*	0.272	α	5.0	1.97	17.4	259	LEG	
1745+6415	7C-III, 8C-NEC, NEC*	0.673	α	2.1	0.59	20.5	44.2	HEG	
1745+6422	7C-III, 8C-NEC, NEC*	1.23	α	5.2	1.41	21.9	138	WQ	
1745+6624	7C-III	3.01	β	1.0	0.51	-	<3.6	NLG	$K = 20.2$
1747+6533	7C-III, 8C-NEC, NEC*	1.516	α	7.3	2.72	21.8	5.6	WQ	
1748+6703	7C-III, 8C-NEC, NEC*	?	-	7.5	2.17	23.9	-	?	
1748+6657	7C-III, NEC*	1.045	β	<0.8	1.15	22.4	2.6	NLG	
1748+6731	7C-III, 8C-NEC, NEC*	0.56	α	1.8	0.64	19.9	803	HEG?	
1751+6809	7C-III, 8C-NEC, NEC*	1.54	β	2.4	1.03	22.9	17.1	NLG	
1750+6805	8C-NEC	?	-	1.3	0.35	>23.2	-	?	8C1751+681C
1751+6741	8C-NEC, NEC*	1.43	γ	1.9	0.33	22.8	32.6	NLG	
1751+6455	7C-III, 8C-NEC, NEC*	0.294	α	1.8	0.65	17.1	234	LEG	
1753+6311	7C-III, 8C-NEC, NEC*	1.96	γ	4.4	1.06	22.6	140	NLG	
1753+6627	8C-NEC	?	-	1.4	0.32	>23.6	-	?	
1753+6543	7C-III, 8C-NEC, NEC*	0.140	α	4.6	1.62	17.2	272	WQ	
1754+6420	7C-III, 8C-NEC, NEC*	1.09	β	2.0	0.50	>22.4	129	NLG	
1754+6311	8C-NEC	1.23	α	1.8	0.44	21.1	215	WQ	
1755+6314	7C-III, 8C-NEC, NEC*	0.388	α	4.8	1.19	18.0	254	LEG	FRI
1755+6830	7C-III, 8C-NEC, NEC*	0.744	α	3.8	1.11	20.0	72.1	NLG	
1756+6520	7C-III, 8C-NEC, NEC*	1.48	γ	2.6	0.67	>23.4	39.4	NLG	
1757+6741	8C-NEC	1.31	β	1.5	0.39	22.3	155	WQ	
1758+6535	7C-III, 8C-NEC, NEC*	0.80	α	3.3	1.13	22.0	872	NLG	
1758+6553	7C-III, 8C-NEC, NEC*	0.171	α	3.7	1.30	16.8	434	LEG	
1758+6307	7C-III, 8C-NEC, NEC*	1.19	α	4.9	1.86	21.1	29.3	WQ	
1758+6719	7C-III, 8C-NEC, NEC*	2.70	α	2.0	0.76	23.6	340	NLG	
1801+6902	7C-III, 8C-NEC, NEC*	1.27	α	4.1	1.37	19.4	181	Q	
1802+6456	7C-III, 8C-NEC, NEC*	2.11	α	9.9	1.97	22.8	211	NLG	
1803+6605	8C-NEC, NEC*	1.61	α	2.3	0.44	21.1	306	WQ?	
1804+6625	7C-III, 8C-NEC	1.91	α	1.4	0.55	20.2	33.1	Q	
1804+6313	7C-III, 8C-NEC, NEC*	?	-	3.1	0.62	23.0	-	?	
1805+6332	7C-III, 8C-NEC, NEC*	1.84	α	5.4	1.04	>23.7	117	NLG	
1807+6831	7C-III, 8C-NEC, NEC*	0.58	α	7.0	2.12	19.9	218	HEG	
1807+6719	7C-III	2.78	α	1.0	0.71	>23.5	14.2	NLG	
1807+6841	7C-III, 8C-NEC, NEC*	0.816	α	2.3	0.60	22.0	99.2	NLG	
1807+6743	8C-NEC	?	-	2.0	0.36	21.6	-	?	
1811+6321	7C-III, 8C-NEC, NEC*	0.273	γ	3.0	0.95	19.3	270	LEG	
1812+6814	7C-III	1.08	α	1.2	0.59	22.5	189	NLG	
1813+6846	7C-III, 8C-NEC, NEC*	1.03	α	4.6	1.51	19.3	444	Q	
1813+6439	7C-III, 8C-NEC, NEC*	2.04	α	1.9	0.50	22.0	310	WQ	
1814+6702	7C-III, 8C-NEC, NEC*	4.05	γ	8.0	2.26	24.1	115	NLG	
1814+6550	8C-NEC	0.95	β	1.3	0.47	20.0	22.9	Q	
1814+6529	7C-III, 8C-NEC, NEC*	0.96	β	4.7	1.22	22.8	1069	NLG	
1815+6805	7C-III, 8C-NEC, NEC*	0.230	α	5.9	1.96	17.8	233	WQ	
1815+6815	7C-III, 8C-NEC, NEC*	0.794	α	3.8	1.37	20.8	1643	NLG	

Table 9. Complete listing of the samples continued

Object	Samples	z	grade	S_{38} /Jy	S_{151} /Jy	R	Size /kpc	Class	Notes
1816+6710	7C-III, 8C-NEC, NEC*	0.92	γ	3.6	2.36	>23.8	16.0	NLG	$H = 18.8$
1816+6605	7C-III, 8C-NEC, NEC*	0.92	β	3.8	1.29	22.3	228	NLG	
1819+6550	7C-III, 8C-NEC, NEC*	0.724	α	2.8	1.17	21.6	68.3	NLG	
1820+6657	7C-III	2.98	γ	<0.8	0.83	>24.1	<3.6	NLG	
1821+6442	Excluded	?	-	2.5	0.82	-	-	?	Bright star at ID position
1821+6419A	8C-NEC, NEC*	0.298	α	1.8	0.48	14.1	110	RQQ	E1821+643
1821+6419B	8C-NEC	0.304	$\alpha?$	1.6	0.40	18.1	36.7	LEG?	FRI in cluster with E1821+643
1822+6601	7C-III, 8C-NEC, NEC*	0.37	α	2.5	0.97	18.7	322	LEG	
1825+6602	7C-III, 8C-NEC, NEC*	2.38	γ	2.1	0.84	23.4	<7.8	NLG	
1826+6510	7C-III, 8C-NEC, NEC*	0.646	α	3.0	1.39	20.7	265	LEG	
1826+6704	7C-III, 8C-NEC, NEC*	0.287	α	1.3	0.60	17.8	102	WQ?	
1827+6709	7C-III, 8C-NEC, NEC*	0.48	β	2.7	1.10	21.0	119	LEG	
1827+6517	Excluded	?		3.1	0.78	-	-	?	Bright star at ID position

Note: the R -magnitudes are measured in a 63-kpc metric aperture, limits are 3σ .

(a)

(b)

Figure 8. Size vs spectral index for (a) the NEC* + 3C* samples, and (b) the 7C-III + LRL samples. Crosses are 3C* in (a) and LRL in (b), filled circles are NEC* in (a) and 7C-III in (b). Note the larger number of small, flatter spectrum objects in the 7C-III+LRL sample compared to the NEC*+3C* sample.

in η of < 0.1 . The new selection criteria are effective at removing CSS objects, most of which seem to show a flattening in their spectra at low frequencies, and therefore emit relatively low power at 151 MHz in the rest frame. This produces a “cleaner” looking correlation, indeed so good that we have felt confident using parametric methods to evaluate the slope of the correlation. The slopes were determined using the Estimation-Maximisation method as implemented in the IRAF task EMMETHOD (Isobe & Feigelson 1990) which is able to deal with the size limits in the data by assuming a normal distribution for the correlation residuals. As only one NEC* and four 7C-III objects had size limits this is unlikely to have affected the correlations.

The correlation slopes for the NEC* + 3C* samples are flatter than the Blundell et al. (1999) values. Though this is only marginally significant statistically, it is clear from examination of Fig. 9 that this effect is due to larger numbers of high redshift CSS sources in the 151-MHz (observed-frame) selected samples. The small size of these objects ($\lesssim 30$ kpc) means that most of them are probably confined by the interstellar medium of the host galaxy, and this high density environment will make the conversion of jet kinetic power into radio emission particularly efficient. A steep jet luminosity function (e.g. Kaiser & Alexander 1998) will then

lead to them being preferentially included in flux-limited samples, particularly at high rest-frame selection frequencies where their spectra are yet to start flattening. For the 7C-III sample we obtain slopes very similar to those of Blundell et al. (probably in part because we use the same LRL sample for comparison). We thus find that the dependence of radio source size on redshift is fairly weak, with radio source size evolving approximately with the scale factor of the Universe, $(1+z)^{-1}$. In particular the upper envelope of the size distribution is very weakly dependent on redshift.

The trend of decreasing size with redshift has usually been assumed to be a straightforward consequence of increasing environmental density with redshift, combined with a finite source lifetime (e.g. Subramanian & Swarup 1990). However, the strong selection pressures associated with the steep radio luminosity function mean that what is being measured is the size at which, for a given redshift, the average radio source reaches its maximum luminosity. Hence if, as argued by Blundell et al. (1999), high redshift, high luminosity sources reach their maximum luminosities earlier in their lives than low redshift ones due to a combination higher inverse-Compton losses and a correlation of injection spectral index with radio luminosity, this is also a possible explanation. Recently, Kaiser & Alexander (1998) have also

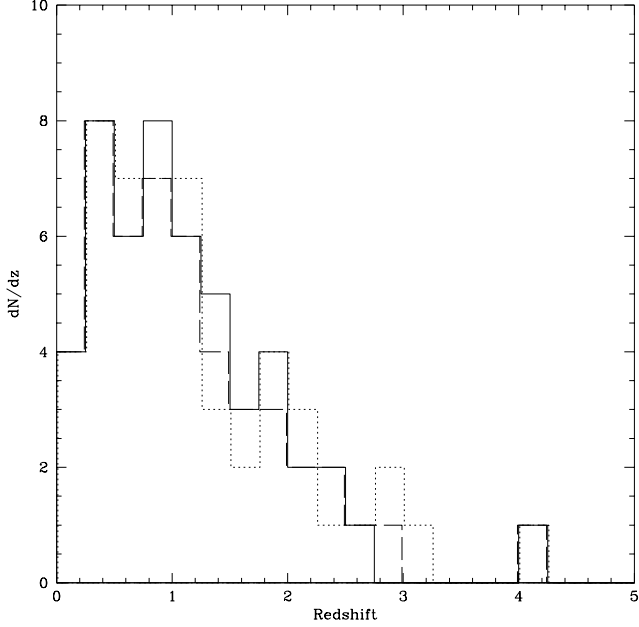


Figure 7. The comparative redshift distributions of the 8C-NEC, 7C-III and NEC* samples. The 8C-NEC sample is the solid histogram, the short-dash the 7C-III and the long-dash the NEC*.

suggested that if either the lifetimes of radio sources or the shape of the density distribution of their environments affects the powers of the jets they can explain both the epoch dependence of linear size and the rapid evolution in the luminosity function of the FR II population, at least within 3C. One observational way in which modelling uncertainties could be addressed is by finding “dead” radio sources and estimating their ages; this may be the only way of constraining whether finite source lifetimes are likely to play an important rôle in evolutionary scenarios.

The influence of the CSS sources in driving the redshift-size correlation in flux-density limited samples of FR II radio sources could explain why much steeper slopes are seen when samples are selected at higher frequency, because these samples typically contain substantially larger fractions of CSS sources than LRL. The CSS sources could also account for the radio luminosity dependence too. The most likely mechanisms for spectral flattening (thermal absorption; Bicknell et al. 1997, or synchrotron self-absorption) are both likely to be luminosity dependent, thermal absorption through the emission line luminosity – radio luminosity correlation and synchrotron self-absorption more directly. Kapahi (1989) removed CSS sources from his study of size evolution, and found that the best-fit value of η was reduced (from 3.5 ± 0.5 to 2.5 ± 0.5) and the dependence on luminosity was weakened (ϵ was reduced from 0.4 ± 0.1 to 0.2 ± 0.1). These correlations are still steeper than we observe for the NEC* + 3C* sample ($\eta = 1.6 \pm 0.3$, $\epsilon \approx 0$), although the errors on the slopes both in our study and that of Kapahi’s are sufficient for the discrepancies to be due to a combination of statistical fluctuations and the lack of spectroscopic redshift completeness in the samples used by Kapahi in particular.

Table 10. The $\lg D - \lg(1+z)$ correlations for the NEC* and 7C-III samples

α, β & γ redshifts		Correlation exponent, η	
Cosmology		NEC* + 3C*	7C-III + LRL
$\Omega_M = 1, \Omega_\Lambda = 0$		1.60 ± 0.29	2.09 ± 0.29
$\Omega_M = 0, \Omega_\Lambda = 0$		1.17 ± 0.29	1.66 ± 0.29
$\Omega_M = 0.1, \Omega_\Lambda = 0.9$		1.07 ± 0.29	1.57 ± 0.29
α redshifts only		Correlation exponent, η	
Cosmology		NEC* + 3C*	
$\Omega_M = 1, \Omega_\Lambda = 0$		1.29 ± 0.30	
$\Omega_M = 0, \Omega_\Lambda = 0$		0.88 ± 0.30	
$\Omega_M = 0.1, \Omega_\Lambda = 0.9$		0.74 ± 0.30	

ACKNOWLEDGEMENTS

We would like to thank Christian Kaiser and Jasper Wall for their helpful comments on the manuscript, and Malcolm Bremer, Rob van Ojik and Richard Saunders for assistance during the 1993 June WHT observations. We also thank the staff at the WHT, McDonald Observatory, Lick Observatory and the IRTF for their assistance. The WHT is operated on the island of La Palma by PPARC in the Spanish Observatorio del Roque de los Muchachos of the Instituto de Astrofísica de Canarias. SER was a visiting astronomer at the NASA Infrared Telescope Facility, operated by the University of Hawaii under contract with NASA. Offset star positions were obtained using astrometry from the guide stars selection system astrometric support system (GASP), developed at the Space Telescope Science Institute, which is operated by the Association of Universities for Research in Astronomy, Inc. for NASA. This research has made use of the NASA/IPAC Extragalactic Database (NED) which is operated by the Jet Propulsion Laboratory, California Institute of Technology, under contract with the National Aeronautics and Space Administration.

APPENDIX A: THE 3C* SAMPLE

To select a bright comparison sample in a similar manner to the NEC* sample we used data from two 38 MHz surveys to obtain low frequency flux densities for radio sources in the sample of LRL, resulting in two different flux density limits. In the region covered by the 38-MHz survey of Rees (1990) we used $S_{151(\text{rest})}/(1+z) \geq 12$ Jy, and in the remainder of the northern sky, $S_{151(\text{rest})}/(1+z) \geq 15$ Jy using flux density from the 38-MHz survey of Williams, Kenderdine & Baldwin (1966) corrected according to Laing & Peacock (1980). Flux densities at higher frequencies were mostly obtained from Laing & Peacock (1980). The members of the sample are listed in Table A1, and those of the NEC* sample in Table A2.

The redshift distributions of the LRL and 3C* samples are not significantly different statistically; a Kolmogorov-Smirnov test on the two samples gives a probability of 18 per cent that they are drawn from the same underlying distribution. There does, however, seem to be a relative lack of high redshift objects in the 3C* sample due to the CSS sources dropping out (Fig. A1).

(a) (b)

Figure 9. The size-redshift relation (a) for sources in the NEC* and 3C* samples and (b) the 7C-III and LRL samples, plotted for $\Omega_M = 0.1$, $\Omega_\Lambda = 0.9$. Objects in the brighter samples are plotted as stars and objects in the fainter as squares. The dashed lines show the best fitting lines from Table 6.

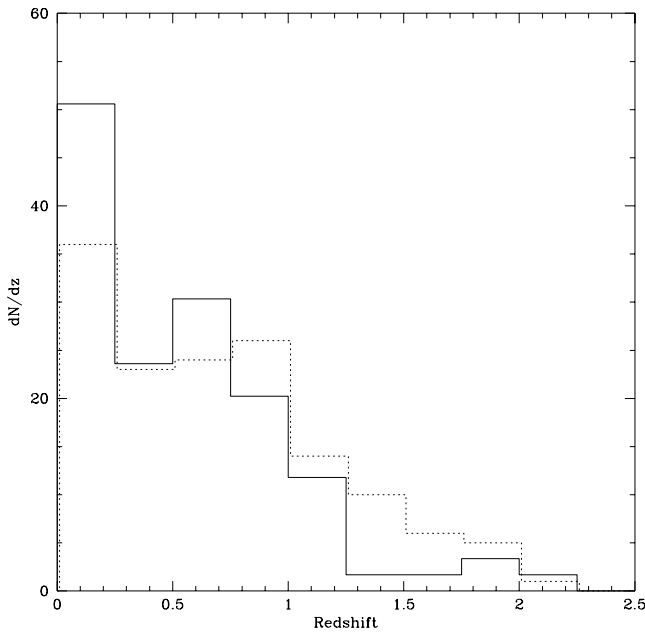


Figure A1. Redshift distributions for LRL (dashed) and 3C* (solid). Note that the 3C* redshift distribution has been multiplied by 1.7 to normalise to the number of objects in LRL.

REFERENCES

- Alexander P., Leahy J.P., 1987, MNRAS, 225, 1
 Baum S.A., O'Dea C.P., de Bruyn A.G., Murphy D.W., 1990, A&A, 232, 19
 Becker R.H., White R.L., Edwards A.L., 1991, ApJS, 75, 1
 Benítez N., Martínez-González E., Martín-Mirónes J.M., 1997, A&A, 321, L1
 Bicknell G.V., Dopita M.A., O'Dea C.P., 1997, ApJ, 485, 112
 Blundell K.M., Willott C.J., Rawlings S., 1999, AJ, 117, 677
 Dey A., Spinrad H., Dickinson M., 1995, ApJ, 440, 515
 Dunlop J.S., Peacock J.A., 1990, MNRAS, 247, 19
 Eales S.A., 1985, MNRAS, 217, 149
 Eales S.A., Rawlings S., Law-Green D., Cotter G., Lacy M., 1997, MNRAS, 291, 593
 Gregory P.C., Condon J.J., 1991 ApJS, 75, 1011
 Isobe T., Feigelson E.D., 1990, BAAS, 22, 917
 Jackson N., Rawlings S., 1997, MNRAS, 286, 241
 Kaiser C.R., Alexander P., 1999, MNRAS, 302, 515
 Kaiser C.K., Schoenmakers A.P., Röttgering H.J.A., 1998, MNRAS, submitted
 Kassim N.E., 1989, ApJ, 347, 915
 Kapahi V.K., 1989, AJ, 97, 1
 Kollgaard R.I., Brinkman W., Chester M.M., Feigelson E.D., Hertz P., Reich P., Wielebinski R., 1994, ApJS, 93, 145
 Kollgaard R.I., Feigelson E.D., Laurent-Muehleisen S.A., Spinrad H., Dey A., Brinkmann W., 1995, ApJ, 449, 61 (K95)
 Lacy M., Rawlings S., Warner P.J., 1992, MNRAS, 256, 404 (Paper I)
 Lacy M., Hill G.J., Kaiser M.E., Rawlings S., 1993, MNRAS, 263, 707 (Paper II)
 Lacy M., et al., 1994, MNRAS, 271, 504
 Lacy M., Riley J.M., Waldram E.M., McMahon R.G., Warner P.J., 1995, MNRAS, 276, 614
 Lacy M., 1998, in: Röttgering H.J.A., Best P.N., Lehnert M.D., eds, "The most distant radio galaxies". Royal Netherlands Academy of Arts and Sciences, Amsterdam, p. 437
 Lacy M., Kaiser M.E., Hill G.J., Rawlings S., Leyshon G., 1999a, MNRAS, in press (Paper III)
 Lacy M., Blundell K.M., Hill G.J., Kaiser M.E., Rawlings S., 1999b, in preparation
 Lacy M., Ridgway S.E., Wold M., Lilje P.B., Rawlings S., 1999c, MNRAS, in press (LRWLR)
 Laing R.A., Peacock J.A., 1980, MNRAS, 190, 903
 Laing R.A., Riley J.M., Longair M.S., 1983, MNRAS, 204, 151 (LRL)
 Loiseau N., Reich W., Wielebinski R., Reich P., Münch W., 1988, A&AS, 75, 67
 McCarthy P.J., 1993, ARA&A, 31, 639
 Neeser M.J., Eales S.A., Law-Green J.D., Leahy J.P., Rawlings S., 1995, ApJ, 451, 76
 Oort M.J.A., Katgert P., Windhorst R.A., 1987, Nat, 328, 500
 Owsianik I., Conway J.E., Polatidis A.G., 1998, A&A, 336, L370
 Rawlings S., Lacy M., Blundell K.M., Eales S., Bunker A., Garington S.T., 1996, Nat, 383, 502
 Rees N., 1990, MNRAS, 244, 233
 Rengelink R.B., Tang Y., de Bruyn A.G., Miley G.K., Bremer M.N., Röttgering H.J.A., Bremer M.A.R., 1997, A&AS, 124, 259
 Scheuer P.A.G., 1995, MNRAS, 277, 331
 Schoenmakers A.P., 1999, A&A, 341, 44
 Subramanian K., Swarup G., 1990, MNRAS, 247, 237
 van Ojik R., Röttgering H.J.A., Miley G.K., Bremer M.N., Macchetto F., Chambers K.C., 1994, A&A, 289, 54
 Williams P.J.S., Kenderdine S., Baldwin J.E., 1966, Mem. R. astr. Soc., 70, 53
 Willott C.J., 1998, D. Phil. thesis, University of Oxford

Table A1. The FR II sources in the 3C* sample with rest-frame flux densities at 151 MHz and rest-frame spectral indices at 1 GHz

Name	redshift	S_{151} (rf) /Jy	$\alpha_{1\text{GHz}}$ (rf)	Type	radio size /arcsec
3C6.1	.8404	25.6	0.77	HEG	26.0
3C9	2.0120	63.8	1.04	Q	14.0
3C20	.1740	59.5	0.75	HEG	53.0
3C28	.1952	27.1	1.18	LEG	52.0
3C33	.0595	66.8	0.73	HEG	253.0
3C33.1	.1810	19.9	0.86	WQ	227.0
3C34	.6900	28.4	1.04	HEG	48.0
3C35	.0670	17.5	0.88	LEG	730.0
3C47	.4250	50.1	0.99	Q	69.0
3C55	.7350	42.7	0.98	HEG?	71.0
3C61.1	.1860	42.8	0.83	LEG	185.0
3C68.2	1.5750	47.9	1.23	HEG?	22.3
3C79	.2559	42.7	0.95	HEG	87.0
3C98	.0306	56.6	0.69	HEG	310.0
3C109	.3056	32.0	0.87	WQ	90.0
3C123	.2177	290.3	0.78	LEG	40.0
3C132	.2140	21.0	0.80	LEG	23.0
3C147	.5450	74.6	0.57	Q	3.0
3C153	.2769	22.9	0.76	HEG	8.5
3C172	.5191	24.8	0.86	HEG	103.0
3C173.1	.2920	23.5	0.91	LEG	60.0
3C175	.7680	41.2	1.03	Q	48.0
3C184	.9900	24.9	0.87	HEG	4.8
3C184.1	.1182	18.1	0.76	HEG	167.0
3C186	1.0630	34.9	1.14	Q	100.0
DA240	.0350	29.8	0.83	LEG	2164.0
3C192	.0598	29.6	0.74	HEG	196.0
3C196	.8710	124.3	0.80	Q	10.0
3C200	.4580	22.1	0.94	LEG	26.0
3C204	1.1120	28.8	1.08	Q	35.0
3C207	.6840	26.4	0.83	Q	14.0
3C208	1.1100	43.2	1.05	Q	11.0
3C216	.6680	38.2	0.99	Q	30.0
3C219	.1744	59.3	0.89	WQ	189.0
3C220.1	.6100	28.8	1.01	HEG	30.0
3C220.3	.6850	30.6	0.95	HEG	7.4
3C223	.1368	20.4	0.76	HEG	303.0
3C225B	.5820	32.0	0.92	HEG?	4.6
3C226	.8177	31.1	0.95	HEG	35.0
4C73.08	.0581	19.8	0.92	HEG	947.0
3C228	.5520	32.3	0.85	HEG	45.0
3C234	.1848	48.8	0.96	WQ	110.0
3C239	1.7900	44.5	1.07	HEG	11.2
3C244.1	.4280	36.1	0.91	HEG	53.0
3C249.1	.3110	18.6	0.87	Q	44.0
3C252	1.1050	35.7	1.12	HEG	60.0
3C254	.7340	38.2	0.96	Q	13.1
3C263	.6563	28.1	0.85	Q	44.2
3C263.1	.8240	33.6	0.90	HEG	6.8
3C265	.8108	44.6	1.02	HEG	78.0
3C267	1.1420	32.6	0.90	HEG	38.0
3C268.1	.9737	39.3	0.64	HEG	46.0
3C274.1	.4220	28.7	0.94	HEG	150.0
3C275.1	.5570	30.5	0.94	Q	18.0
3C277.2	.7660	26.7	0.96	HEG	58.0
3C280	.9960	46.0	0.79	HEG	14.5
3C292	.7130	22.7	0.86	HEG	133.0
3C293	.0452	20.5	0.69	LEG?	216.0
3C294	1.7800	45.2	1.11	HEG	15.0
3C295	.4614	98.8	0.70	HEG	5.3
3C300	.2700	29.4	0.88	HEG	100.0
3C309.1	.9040	39.4	0.76	Q	2.9
3C310	.0540	86.3	1.20	LEG?	310.0
3C319	.1920	22.1	0.97	LEG	105.0

Table A1. continued

Name	redshift	S_{151} (rf) /Jy	$\alpha_{1\text{GHz}}$ (rf)	Type	radio size /arcsec
3C321	.0960	23.7	0.84	HEG	290.0
3C324	1.2063	37.3	0.93	HEG	10.0
3C326	.0895	26.3	0.84	LEG	1190.0
3C325	.8600	27.6	0.80	Q	16.0
3C330	.5490	48.4	0.77	HEG	62.0
3C334	.5550	25.3	0.95	Q	58.0
3C349	.2050	20.7	0.79	HEG	82.0
3C351	.3710	21.5	0.75	Q	65.0
4C13.66	1.4500	40.2	1.07	HEG	6.0
3C368	1.1320	41.6	1.24	HEG	7.9
3C380	.6910	127.1	0.83	Q	20.0
3C381	.1605	21.0	0.76	HEG	69.0
3C382	.0578	27.6	0.74	WQ	189.0
3C388	.0908	33.5	0.84	HEG	43.0
3C390.3	.0569	62.4	0.77	WQ	215.0
3C401	.2010	29.3	0.84	LEG	24.0
3C427.1	.5720	49.4	0.99	LEG	23.1
3C436	.2145	26.3	0.89	HEG	104.0
3C438	.2900	68.9	1.02	HEG	22.0
3C442A	.0263	26.3	0.99	LEG	590.0
3C452	.0811	73.5	0.89	HEG	250.0
3C457	.4270	23.4	1.03	HEG	190.0

Willott C.J., Rawlings S., Blundell K.M., Lacy M., 1998, MN-
RAS, 300, 625

Willott C.J., Rawlings S., Blundell K.M., Lacy M., Eales S., 1999,
MNRAS, in press

Table A2. The FRII and probable FRII sources in the NEC* sample with rest-frame 151 MHz flux densities and rest-frame 1 GHz spectral indices

Name	redshift	S_{151} (rf) /Jy	$\alpha_{1\text{GHz}}$ (rf)	radio size /arcsec
1732+6535	0.856	9.87	0.82	20.0
1733+6719	1.84	4.46	0.87	2.5
1736+6504	2.40	2.25	1.28	17.0
1741+6704	1.054	1.23	0.96	3.9
1742+6346	1.27	1.41	0.97	51.0
1743+6344	0.324	1.79	0.83	14.0
1743+6431	-	-	-	45.0
1743+6639	0.272	2.39	0.71	50.0
1745+6415	0.673	1.00	0.69	5.6
1745+6422	1.23	3.27	0.95	16.0
1747+6533	1.516	5.80	0.85	0.7
1748+6703	-	-	-	14.0
1748+6657	1.045	1.24	0.42	0.3
1748+6731	0.56	0.91	0.78	108.0
1751+6809	1.54	1.68	0.77	2.0
1751+6741	1.43	1.13	1.39	3.8
1751+6455	0.294	0.86	0.79	43.0
1753+6311	1.96	3.16	0.96	17.0
1753+6543	0.140	1.93	0.67	84.0
1754+6420	1.09	0.99	0.88	15.0
1755+6830	0.744	1.97	0.87	8.9
1756+6520	1.48	1.48	0.79	4.6
1758+6535	0.80	1.81	0.74	106.0
1758+6553	0.171	1.54	0.90	115.0
1758+6307	1.19	3.39	0.81	3.4
1758+6719	2.70	1.91	0.85	45.0
1801+6902	1.27	2.75	0.97	21.0
1802+6456	2.11	6.67	1.03	26.0
1803+6605	1.61	1.30	1.07	36.0
1804+6313	-	-	-	29.0
1805+6332	1.84	3.50	0.96	14.0
1807+6831	0.58	3.27	0.84	29.0
1807+6841	0.816	1.09	0.82	12.0
1811+6321	0.273	1.12	0.87	52.0
1813+6846	1.03	2.67	0.88	52.0
1813+6439	2.04	1.58	1.07	38.0
1814+6702	4.05	10.98	0.98	18.0
1814+6529	0.96	2.44	1.02	126.0
1815+6805	0.230	2.50	0.91	50.0
1815+6815	0.794	2.12	0.93	200.0
1816+6710	0.92	3.00	0.75	27.0
1816+6605	0.92	2.24	0.93	1.9
1819+6550	0.724	1.71	0.73	8.5
1822+6601	0.37	1.29	0.81	52.0
1825+6602	2.38	2.72	0.83	<1.0
1826+6510	0.63	1.91	0.83	34.0
1826+6704	0.287	0.71	0.75	19.0
1827+6709	0.48	1.45	0.85	17.0

